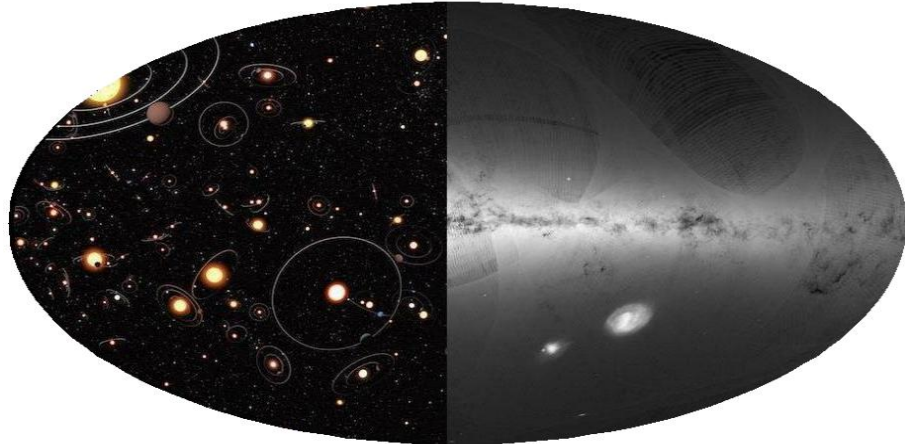


ON THE SEARCH FOR EXO-RINGS IN GAIA DATA



MAJOR RESEARCH PROJECT IN ASTRONOMY

Presented by:

JORGE ANDRÉS VILLA VÉLEZ

To obtain the MSc. Astronomy degree

Under the supervision of

Dr. A.G.A. Brown

Dr. M.A. (Matthew) Kenworthy

Second Reader

Dr. blah blah blah



**Universiteit
Leiden**
Sterrewacht Leiden

Universiteit Leiden - Sterrewacht Leiden
Faculteit Wiskunde en Natuurwetenschappen
2018

ABSTRACT

Nlah blah

Key words:*Submillimeter galaxies - (SMGs), ALESS-survey, CO line emission, Spectroscopic redshift, Molecular mass.*

*Wat mij betreft weet ik niets zeker,
maar naar de sterren kijken zet me aan het dromen.*

—Vincent Willem van Gogh
(1853 – 1890) Dutch Post-Impressionist painter.

*It is sometimes said that scientists are unromantic,
that their passion to figure out robs the world of beauty and mystery.
But is it not stirring to understand how the world actually works —that white light is made of
colors, that color is the way we perceive the wavelengths of light,
that transparent air reflects light, that in so doing it discriminates among the waves,
and that the sky is blue for the same reason that the sunset is red?
It does no harm to the romance of the sunset to know a little bit about it.*

—Carl Sagan, Pale Blue Dot: A Vision of the Human Future in Space
(1935 - 1996) American astronomer, cosmologist, astrophysicist, astrobiologist, author, science popularizer, and science
communicator in astronomy and other natural sciences.

*In third Dialogue there is first denied that base illusion of the shape of the heavens, of their
spheres and diversity.
For the heaven is declared to be a single general space, embracing the infinity of worlds,
though we do not deny that there are other infinite 'heavens' using that word in another sense.
For just as this earth hath her own heaven (which is her own region), through which she moveth
and hath her course,
so the same may be said of each of the innumerable other worlds..*

—Giordano Bruno
(1548 – 1600) Italian Dominican friar, philosopher, mathematician, poet, and cosmological theorist.

ACKNOWLEDGMENTS

First and foremost I would like to thank my amazing supervisors, Dr. A.G.A. Brown and Dr. M.A. (Matthew) Kenworthy, who encouraged me to research in a completely different fashion, in a branch of Astronomy I had never worked on as it is the exoplanets and the Gaia mission. I am extremely grateful for all the new things they taught me in order to be a good researcher and to pave my way as a scientist.

To my parents, Jorge Mario Villa Marín and Gladys Vélez Muñoz who have trusted in me through this years, always supporting all my dreams and also now in this adventure. They have always been an important shoulder I can rely on to take every step forward on my way to be a good scientist. To all my family in Colombia and USA because this dream would have not been becoming real without their enormous help and trust in me.

Also, to Paula Andrea Ortíz Otálvaro who helped me to get rapidly involved in the Dutch life-style and feel Leiden as a second home since the first day. To my fellow master Colombian friends Juan Manuel Espejo Salcedo and Andrés Felipe Ramos Padilla for all those good times lived inside

and outside the university. For all those enriching talks which shed light when problems seemed to have no solution. Someone, who motivated me to study and to look forward, Guadalupe Cañas Herrera, my little Spanish friend, thanks for all those good advises and funny times.

My dutch friends which helped me to feel this country as a second home, for all those good times and memories that will be forever in my mind (Michelle Willebrands, Esmee Stoop, Charlotte Brand, Lieke van Son, Marco Trueba van den Boom, Job van der Wardt, Dennis Vaendel, Lennart van Sluijs, Martijn Oei and Dirk van Dam). I would also like to dedicate this to my fellow international master friends who came here to make the same dream come true, Louis Martin, Michail Dagtzis and Pranav Kumar Mohanty. Last but not least, to Sofia Sarperi and Riccardo Mattia Baldo which I had the pleasure to meet during their Erasmus program in Leiden. To them, a big thank for all the good moments and conversations.

When I arrived to Leiden I thought it was going to be impossible to keep on doing the things I used to in Medellín. However I met a group of beautiful people who accepted me and shared all their empathy with me. To the Chileans Valeria Olivares, Pedro Salas, Pablo Castellanos, Heather Andrews, Javiera Paz, Sebastián Rumie and Nicolás Salinas. Also to my Mexican friend Santiago Torres, my Colombian friends Lina Bayona and Diana Aranzales who always took care of me. To one person who was always there to support and encourage me, my Portuguese friend Marta Figueiredo. To Dennis Hiltrop the kindest German I have ever met, with whom I had enriching talks. To Kathy Fourment with who I had really nice talks and funny days.

Before coming to The Netherlands I was going through a bad time and now that I am here witnessing this dream coming true I really need to thank to my cousin Jaime Muñoz and his husband William Lundquist because they took care of me while in California during one of my darkest times, helping and cheering me up when needed. They always encouraged me to continue straight on the science path, being humble and never backing off.

To all the people who directly or indirectly made this first step on my way to get a master in Astronomy possible, many many thanks and I will keep on fighting until the end on my way to keep on reaching my dreams.

CONTENT

1	THEORETICAL FRAMEWORK	1
1.1	Introduction	1
1.2	Exo-Rings	2
1.3	Gaia mission	2
1.4	Sco-Cen	2
2	MODEL AND SAMPLES	3
2.1	Introduction	3
2.2	Power Law Distributions	3
2.3	Exoplanets: Period-Mass Distributions	4
2.3.1	β -istribution	5
2.3.2	Single Power-Law	6
2.4	Stellar Mass Distribution	7
2.4.1	Salpeter Power-Law	7
2.4.2	Kroupa Power-Law	7
2.5	Probability of Transit Detection	8
2.5.1	Geometry of the Transit	10
2.5.2	Rings Lifetime	13
2.6	Monte-Carlo simulations	14
2.7	Detection Probability: Monte-Carlo vs Analytic Form	18
3	GAIA AND SUPERWASP SAMPLE DATA	29
3.1	Introduction	29
3.2	Sco-Cen OB Association	29
3.3	Gaia Samples	29
3.4	Stellar Evolution Models	30
3.5	Light Curves	34
4	RESULTS AND DISCUSSION	37
4.1	Introduction	37
5	SUMMARY	39
	BIBLIOGRAPHY	41
6	APPENDIX	45
6.1	SQL-queries	45
6.2	Sample selection	46

LIST OF FIGURES

Figure 1	Something!	11
Figure 2	Something!	12
Figure 3	Something!	12
Figure 4	Something!	15
Figure 5	Something!	15
Figure 6	Something!	16
Figure 7	Something!	17
Figure 8	Something!	18
Figure 9	Something!	19
Figure 10	Something!	19
Figure 11	Something!	20
Figure 12	Something!	21
Figure 13	Something!	22
Figure 14	Something!	23
Figure 15	Something!	24
Figure 16	Something!	25
Figure 17	Something!	26
Figure 18	Something!	27
Figure 19	Something!	31
Figure 20	Something!	32
Figure 21	Something!	32
Figure 22	Something!	33
Figure 23	Something!	33
Figure 24	Something!	34
Figure 25	Something!	35
Figure 26	Something!	35
Figure 27	Something!	36
Figure 28	Something!	47
Figure 29	Something!	47

LIST OF TABLES

THEORETICAL FRAMEWORK

1.1 INTRODUCTION

During the last years, the exo-planetary astrophysics field has been getting stronger and stronger. Searching for new worlds revolving around other stars have imposed important challenges in current science such as planetary formation models, observational and instrumentation challenges, for example. With the arrival of new instruments, each time more powerful, Astronomers are able to study and characterize these distant worlds and lately compare them with our solar system. In despite of it, we still have a long way to go in studying and understanding these interesting objects.

This project is mainly focused on studying exo-planets with rings around young stars. At the moment, there is a lot of debate on whether or not, we have observed some features in light curves which could be explained by transiting exo-rings in front of a parent star. On top of that, it is well-known that rings are not an exception in our solar system, where we can observe majestic structures as Saturn's rings or modest ones as the other gaseous-planets. As there is no clear consensus at what time exactly during the stellar life and planetary formation these objects could be formed, we aimed to enhance our chance of detecting these structures while studying young stars. These particular stellar population is expected to be forming planets at early stages which makes them good candidates in our search. The targeted field is known as Sco-Cen, a really young OB stellar stellar association at a distance of 100 – 100pc from the sun. Sco-Cen is composed of (number of star, or any other information) and it is located between the constellations of Scorpius, Centaurus and Crux in the southern hemisphere.

In addition, all the characterization of astrophysical sources is mainly dependent on the relative distance to the observer. Therefore, aiming for excellent measurements of distance is essential to properly address our study. A few years ago in (year), the *Gaia* mission was launched to measure with high precision the parallax of stars using their proper motion. As *Gaia* samples the whole celestial sphere, and we need as much as possible accurate measurements for stars in Sco-Cen, we decided to use this mission.

In this chapter, a brief introduction to planet-formation and exo-rings is provided. Also, we describe the most relevant features of the *Gaia* mission, and a general description of the Sco-Cen OB association.

1.2 EXO-RINGS

1.3 GAIA MISSION

1.4 SCO-CEN

2

MODEL AND SAMPLES

2.1 INTRODUCTION

2.2 POWER LAW DISTRIBUTIONS

It is well-known that the stellar mass, and planetary mass and period can be described by power laws. As those parameters are essential in our formulation for the probability of exo-rings transits, and the subsequent analysis, we must pay attention to how model samples which can reproduce faithfully the observation.

A power law distribution can be defined as the relative change of two quantities, which are related through a common exponent. In other words, we can predict the change in one of the variables once the exponent and an initial set of values for the second variable are known. Mathematically speaking, we define a power law distribution as [Equation 2.1](#), where N and X are the variables, and α is the exponent relating the relative change between them and it is assumed $\alpha \neq 1$. Generally, the variable N refers to the number of objects one would expect to find in a given interval $x_1 \leq X \leq x_2$, where the variable X in our particular case may refer to the planetary period, planetary mass, stellar mass or any other parameter which we want to study.

$$\frac{dN}{dX} \propto X^{-\alpha} \quad (2.1)$$

Power-laws can consist of a single or multiple exponents relating two or more variables. The easiest case is the single power law which has the mathematical form shown in [Equation 2.1](#). However, the equation lacks of a proportionality constant or normalization constant which must be found with boundary conditions. Therefore, [Equation 2.1](#) can be rewritten in a more general fashion as [Equation 2.2](#), where A corresponds to the normalization constant and can be found using [Equation 2.3](#) with $\gamma = 1 - \alpha$.

$$\frac{dN}{dX} = AX^\alpha \quad ; \quad x_1 \leq X \leq x_2 \quad (2.2)$$

$$A = \int_{x_1}^{x_2} X^{-\alpha} dX = \frac{x_2^{1-\alpha} - x_1^{1-\alpha}}{1-\alpha} = \frac{x_2^\gamma - x_1^\gamma}{\gamma} \quad (2.3)$$

Furthermore, we can define the cumulative distribution function (CDF) $F(X)$, which will give us all the accumulated probability less than or equal to X . It is widely used to determine the probability of an observation being greater than a certain value, or between two values. The CDF will be of great importance in [Section 2.6](#) where the randomly distributed variable is obtained making use of it to generate the real variable. The mathematical form of the CDF is given in [Equation 2.4](#) where the upper limit in the integral x here refers to a value between the upper limit (x_1) and lower limit (x_2) over which one wants to generate the distribution.

$$F(x) = A^{-1} \int_{x_1}^x t^{-\alpha} dt = \frac{x^\gamma - x_1^\gamma}{x_2^\gamma - x_1^\gamma} \quad (2.4)$$

Subsequently, if the random variable is distributed uniformly between 0 and 1, one can generate the real variable by inverting the CDF shown in [Equation 2.4](#) which leads to [Equation 2.5](#). As expected, if one evaluates the last equation in $y = 0$ and $y = 1$ which are the extreme values of the random variable, the result is $x = x_1$ and $x = x_2$ respectively in the real variable.

$$\begin{aligned} y &= F(x) = \frac{x^\gamma - x_1^\gamma}{x_2^\gamma - x_1^\gamma} \\ x &= (y(x_2^\gamma - x_1^\gamma) + x_1^\gamma)^{1/\gamma} \end{aligned} \quad (2.5)$$

The planetary mass-period distribution, and the stellar mass distribution will be generated following the simple power law explained above with a Monte-Carlo process in [Section 2.6](#). Although a different method was also explored for the planetary mass-period distribution due to a possible weakly dependence in both parameters ([Jiang et al.,2007](#); [Zucker and Mazeh,2002](#)), we decided to kept the power law method to model them as it is also widely used and studied in literature ([Nielsen et al.,2010](#); [Cumming et al.,2008](#); [Butler et al.,2006](#)).

2.3 EXOPLANETS: PERIOD-MASS DISTRIBUTIONS

In order to draw a reliable distribution sample of period and mass for exoplanets, we used two different approaches. The first approach uses the β -distribution because there exists a weakly

correlation between the period and mass of an exoplanet as shown by [Zucker and Mazeh,2002](#) which makes the distribution analysis not suitable to be addressed by two independent power laws that describe the joint period-mass distribution. Alternatively, one can assume that as the correlation is weak, then each variable can be treated as independent and the distributions may be generated using single power laws as it is also widely explored by other authors ([Nielsen et al.,2010](#)). Therefore, as there exists two different forms to address the generation of these distributions, both ways were explored and implemented in this work.

In [Section 2.3.1](#) and [Section 2.3.2](#), the method is widely explained taking into account the different observations and arguments of the former authors.

2.3.1 β -distribution

Using a data set of 66 exoplanets [Zucker and Mazeh,2002](#) suggested a possible correlation between the mass and period. Subsequently [Jiang et al.,2007](#) using a data set of 233 exoplanets supported this idea measuring a positive correlation coefficient of 0.1762. As a result of the positive correlation, describing the distribution as two independent power laws it is not correct, and a new coupled positively correlated function is needed to describe the problem. However, generating this type of distributions needs β -distributed random variables which was not provided until [Magnussen,2004](#) work.

The probability distribution function (pdf) on a finite interval (c,d) , $-\infty < c < d < \infty$, indexed by two positive parameters α and β is given by [Equation 2.6](#), where $B(\alpha, \beta)$ denotes the beta function and can be computed using [Equation 2.7](#).

$$f_{\beta}(x|\alpha, \beta) = \frac{1}{B(\alpha, \beta)} \frac{(x-c)^{\alpha-1} (d-x)^{\beta-1}}{(d-c)^{\alpha+\beta-1}} ; \quad c \leq x \leq d, \quad \alpha > 0, \quad \beta > 0 \quad (2.6)$$

$$B(\alpha, \beta) = \int_0^1 t^{\alpha-1} (1-t)^{\beta-1} dt = \frac{\Gamma(\alpha)\Gamma(\beta)}{\Gamma(\alpha+\beta)} \quad (2.7)$$

Using the correct transformation, the pdf can be written in terms of a normal distributed variable to obtain the standard β -distribution as shown in [Equation 2.8](#) which is a useful form to implement the algorithm provided in [Magnussen,2004](#).

$$f(y|\alpha, \beta) = \frac{1}{B(\alpha, \beta)} y^{\alpha-1} (1-y)^{\beta-1} ; \quad 0 \leq y \leq 1, \quad (2.8)$$

The final distribution for mass and period can be obtained through [Equation 2.9](#), where $(\hat{\alpha}_m, \hat{\beta}_m) = (0.6524, 5.9070)$ and $(\hat{\alpha}_p, \hat{\beta}_p) = (0.3697, 3.8445)$ as a result of applying a Maximum-Likelihood Method to their observational data. The normalization constants in both cases are given by $A_1 = 115.5$ and $A_2 = 11650$, corresponding to the area below the observed histogram distribution for each one of the parameters.

$$\begin{aligned} f_\beta^M &= A_1 f_\beta(m | \hat{\alpha}_m, \hat{\beta}_m) \\ f_\beta^P &= A_2 f_\beta(p | \hat{\alpha}_p, \hat{\beta}_p) \end{aligned} \quad (2.9)$$

In short, the mass and period distributions can be then generated using [Equation 2.8](#) and [Equation 2.9](#) through a Monte-Carlo process. These equations can be read as the probability of a planet to be in a mass range $[M, M + dM]$ and a period range $[P, P + dP]$. The actual upper and lower limits in mass, and period are given by the data set used to derive the normalization constant and the index of the β -distribution. Thus, we can generate samples in mass-period ranges of $0.008 < M(M_j) < 26.7$ and $0.8079 < P(\text{days}) < 6776.1$. The application of this model to our current problem is shown and discussed in [Section 2.6](#).

2.3.2 Single Power-Law

As discussed in [Section 2.2](#) and [Section 2.3.1](#), the planetary mass and period are weakly correlated, so one can ignore that and addressed the problem as independent single power laws. In the past, this has been studied by ([Cumming et al., 2008](#); [Butler et al., 2006](#)) considering the distributions of semimajor axis and planet mass of known radial velocity planets. However, in recent studies, [Nielsen et al., 2010](#) noted that due to a decrease in sensitivity of the radial velocity method with orbital distance the exponent of the distribution must be modified. The single power law distributions in mass, semimajor axis and period are shown in [Equation 2.10](#).

$$\begin{aligned} \frac{dN}{dm} &\propto m^{-1.16} \\ \frac{dN}{da} &\propto a^{-0.61} \\ \frac{dN}{dP} &\propto P^{-0.74} \end{aligned} \quad (2.10)$$

In the same way as stated before, we can interpret the former equation as the number of planets expected to be contained in a mass range $m_1 < m < m_2$, a semimajor axis range $a_1 < a < a_2$, and orbital period $p_1 < p < p_2$. Whereas in the case of β -distributions, the mass and period cover a wide range, here the mass is reduced to a range of $0.5 < M(M_j) < 13$ and an upper cut-off at 75AU which leads to an upper limit of $\sim 650\text{yr}$ in period allowing to study wider planetary orbits.

2.4 STELLAR MASS DISTRIBUTION

Apart from modeling the planetary mass and period, we aimed to obtain in the same fashion the stellar mass distribution. This is known as the initial mass function (IMF) and it is still a wide open question in current Astrophysics. There exists different power laws which try to describe the number of stars expected to lie in a given mass range. In this work, we decided to test two different forms of the IMF namely the Salpeter power law proposed by Edwin Salpeter in 1955 ([Salpeter,1955](#)) and the Kroupa power law proposed by Pavel Kroupa in 2001 ([Kroupa,2001](#)). The main difference between these two formulations resides on the value that each exponent can take according to each mass range in which one could be interested in. The main goal in using these power laws is to faithfully reproduce the actual observed IMF distribution of stars in a given mass range using the Monte-Carlo process technique. In [Section 2.4.1](#) and [Section 2.4.2](#) a brief introduction of the main features for both power laws is given.

2.4.1 Salpeter Power-Law

In 1955, Edwin Salpeter used the observed luminosity function for main-sequence stars in the solar neighborhood assuming that stars off the main-sequence have already burnt up 10% of their hydrogen mass, and also that stars in the solar neighborhood have been created at a uniform rate for the last five billion years to compute the rate of star creation as a function of stellar mass, and the number of stars in each mass range [Salpeter,1955](#). Having said that, he found the power law describing the IMF to follow [Equation 2.11](#), in which ξ_0 is a constant related to the local stellar density and $\alpha = 2.35$. The former equation gives us the number of stars expected to be in a mass range $[M, M + dM]$.

$$\xi(m)\Delta m = \xi_0 \left(\frac{m}{M_\odot} \right)^{-2.35} \left(\frac{\Delta m}{M_\odot} \right) \quad (2.11)$$

As we are interested in using our own mass range, and just make use of the exponent to draw a mass distribution we can rewrite [Equation 2.11](#) into [Equation 2.12](#), and later apply all the steps listed in [Section 2.2](#) to later make use of the Monte-Carlo process and obtain our sample of modeled stars. The proportionality constant can be found once the total number of stars in a mass range $m_1 < m < m_2$ is known, through [Equation 2.3](#).

$$\frac{dN}{dm} \propto m^{-2.35} \quad (2.12)$$

2.4.2 Kroupa Power-Law

On the other hand, in 2001, a different formulation was proposed by Pavel Kroupa in which the main feature is a change in the slope (power-law index) near to $0.08M_\odot$ and $0.5M_\odot$ [Kroupa,2001](#).

In other words, the number of stars expected in a given mass range has different values for the power-law exponent in contrast to Salpeter's law which has only one index. The general form is given by [Equation 2.13](#). One interesting feature of this power law is that 50% of the data generated falls into the mass range $0.01 \leq \frac{m}{M_\odot} \leq 1.0$, and 50% falls into $1.0 \leq \frac{m}{M_\odot} \leq 50.0$.

$$\xi(m) \propto m^{-\alpha_0} = \begin{cases} \alpha_0 = +0.3 \pm 0.7, & \text{if } 0.01 \leq \frac{m}{M_\odot} \leq 0.08 \\ \alpha_0 = +1.3 \pm 0.5, & \text{if } 0.08 \leq \frac{m}{M_\odot} \leq 0.50 \\ \alpha_0 = +2.3 \pm 0.3, & \text{if } 0.50 \leq \frac{m}{M_\odot} \leq 1.00 \\ \alpha_0 = +3.3 \pm 0.7, & \text{if } 1.00 \leq \frac{m}{M_\odot} \end{cases} \quad (2.13)$$

The IMF generation will be addressed in the same fashion as explained above for the Salpeter's power law, where a Monte-Carlo process will be used and the normalization constant will be set to the total number of stars in a mass range $m_1 < m < m_2$.

2.5 PROBABILITY OF TRANSIT DETECTION

One of the main goals in this work is to constrain the probability of detecting an exo-ring transit around young stars using *Gaia* observations. We should start thinking about the possible factors which could affect the most their detectability such as the geometry of the transit, the chance to observe a star with planets around it, the probability of detecting any feature with *Gaia*'s cadence, the time it takes to form a ring around a planet and how long it lasts, or the probability of a given planet to have its Hill sphere filled with some material which could possibly form rings. A few of these probabilities are hard to compute, basically because the only knowledge we have is provided through observations of our own solar system as could be the rings lifetime. However, we can make our best guess and provide at least a lower boundary of the transit probability detection, and lately obtain the number of planets one would expect to observe given some survey features.

First, we decided to constrain our detectability prediction as a product of five independent probabilities as shown in [Equation 2.14](#), where P_1 corresponds to the probability of a given star to have a planet, P_2 gives the probability of a planet to have its Hill sphere filled with material that would coalesce and form rings, P_3 constrains the probability of observing exoplanetary rings transiting in front of their parent star given an observer in the universe, and P_4 the probability of observing at least one transit with *Gaia* in all the mission lifetime. Apart from these four probabilities, we included another one to account for the rings lifetime but it was addressed separately to study how this could affect the overall outcome and is explained in [Section 2.5.2](#).

$$P_{\text{transit}} = P_1 * P_2 * P_3 * P_4 \quad (2.14)$$

On top of that, we can start constructing each probability in terms of their main variables. Firstly, the probability of a star having a planet was set to a value of $P_1 = 0.17$ which means that a star has on average a 17% chance of hosting a planet. This value was set based on [Cas-san et al.,2012](#) work where a statistical analysis of microlensing data was carried out, revealing that around 17% of stars host Jupiter-mass planets from $0.3M_j$ to $10M_j$. If super-Earths or cool-Neptunes are taken into account this probability is higher, however, as was explained in [Section 2.3](#), the Jupiter-mass planets' probability is in the perfect mass range we want to study, thus, we took this value as a reference to start working out the detectability.

Secondly, we proceed to set a value for P_2 or the chance a planet has to have its Hill sphere filled with material able to form planetary rings. The Hill sphere of an object can be defined as a circular region surrounding the object, inside which, the attraction of satellites dominates and can orbit around the main body. Mathematically speaking, if we have two bodies, let's say a star of mass M_\star and a planet of mass m , and orbital semi-major axis a and orbital eccentricity e , then the planet's Hill sphere radius can be approximated by [Equation 2.15](#) as presented in ([Osborn et al.,2017](#); [Rieder and Kenworthy,2016](#)). This equation will be used later in [Section 2.5.1](#) in order to compute the duration of the eclipse in terms of the Hill sphere which is crucial for our probabilistic formulation.

$$R_H \approx a(1 - e) \left(\frac{m}{3M_\star} \right)^{1/3} \quad (2.15)$$

We chose the most optimistic case and set it to one, which corresponds to a 100% chance of having material orbiting around the planet inside the Hill sphere. This is mainly because as we want to study young stars, we expect the planet to be immersed in an environment full of material to form moons or make the planet grow which can create a disk around it and subsequently create the exo-rings. Although this was not based on scientific material present in literature, we consider the best case so given some observations one could constraint it better and lower down this probability.

On the other hand, we have the probabilities associated with the transit and the rings' lifetime. However, this will be explain thoroughly in [Section 2.5.1](#), and [Section 2.5.2](#) so for the moment we can focus on the fourth probability related to the chance of observing at least one transit with *Gaia*. In this case, it is important to have in mind that the number of times a given star is observed in this mission strongly depends on the scanning-law of the instrument. In average, depending on the position in the sky an object can be observed ~ 70 times during the five-year nominal operations phase [Gaia Collaboration et al.,2016](#), thus, if we assume each observation as independent, this represents the number of trials one has to observe a transit around a given object. In other words, the probability will be the product of each trial. One might consider the worst case, namely, not observing the transit, which will be given in terms of the number of trials (n), the *Gaia* mission duration, and the eclipse duration itself. This probability, corresponding to

P_4 in [Equation 2.14](#) is given in [Equation 2.16](#).

$$P_4 = 1 - \left(\frac{\text{Gaia Duration} - \text{Eclipse Duration}}{\text{Gaia Duration}} \right)^n \quad (2.16)$$

The eclipse duration in our case is strongly related to the Hill sphere of the planet as we do not want to compute the probability of detecting a planet in front of its host star but the exo-rings which could be embedded in the Hill sphere of the planet. Therefore, we have to consider the size of the rings which is given by the time it takes those rings to transit in front of the stellar disk times the orbital velocity assumed to be the same as the circular velocity. Thus, $d_{disk} = v_{circ} t_{ecl}$ and $v_{circ} = 2\pi a / P$, with a and P corresponding to the planet's orbital semi-major axis and orbital period. If we consider the Kepler's third law and also assuming the mass of the parent star to be much larger than the planet and exo-rings mass i.e. $M_\star \gg m$, we can rewrite the circular velocity and use it in the disk diameter equation to obtain the duration of the eclipse [Equation 2.17](#) in terms of the orbital period, the planet and exo-rings mass, and a new parameter which tells us what is the fraction of the Hill sphere that the exo-rings disk fills as presented by [Osborn et al., 2017](#). In our particular case we have decided to set $\xi = 0.3$, which means that 30% of the Hill sphere is filled with material which is typical for a prograde rotating disc and it is also known as the stability criterion ([Quillen and Trilling, 1998](#); [Nesvorný et al., 2003](#)).

$$t_{ecl} = \frac{P\xi}{\pi} \left(\frac{m}{3M_\star} \right)^{1/3} \quad (2.17)$$

In the next sub-sections, we present the geometry of the transit and its relation to obtain the probability P_3 . Also the rings lifetime is presented and discussed as we aim to constrain the probability as much as possible and the rings lifetime is crucial in our analysis.

2.5.1 Geometry of the Transit

As was mentioned before, we aim to obtain how likely is to observe exo-rings transiting in front of their host star. Thus, we have to first obtain the transit probability of a planet and extrapolate this result which is the most general case to our particular situation. First of all, let's consider a star which is transited by a planet in the observer's line of sight as shown in [Figure 1](#). Here, a represents the orbital semi-major axis of the planet, and d_\star the stellar disk diameter. The fraction of area on the celestial sphere which is swept out by the shadow of the planet during one orbital period is given by the ratio between the annulus projected onto the celestial sphere and the total superficial area of the celestial sphere given by [Equation 2.18](#) as presented in [Borucki and Summers, 1984](#). However, from the image it is clear that $s = y\theta$ and $d_\star = a\theta$, hence [Equation 2.18](#) can be written as [Equation 2.19](#) and taking the limit when $y \rightarrow \infty$ we can obtain the transit probability shown in [Equation 2.20](#). This takes into account that the observation of the planet and its parent star is performed at random orientations with respect to the inclination angle of

the planet's plane of orbit. Clearly, this probability only depends on the radius of the star and the planet orbital semi-major axis because in this case the planet is just a point-like source and its radius has been neglected. However, in our case we care about the Hill sphere size which is filled with the rings, then we need to change [Equation 2.20](#) slightly.

$$P = \frac{2\pi(a+y)s}{4\pi(a+y)^2} \quad (2.18)$$

$$P = \frac{yd_\star}{2(a+y)a} \quad (2.19)$$

$$P = \frac{d_\star}{2a} = \frac{R_\star}{a} \quad (2.20)$$

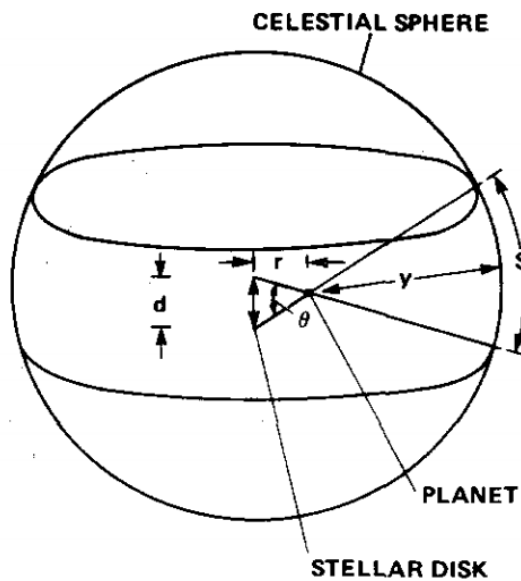


Figure 1: Something!

Now, the transit will not be produced by the point-like source but by its rings as a whole. The geometry for this scenario is shown in [Figure 2](#) where R_\star is the stellar disk radius, a represents the orbital semi-major axis and R_H is the Hill sphere radius. The orbital inclination of $i = 0^\circ$ means the pole is on, whilst $i = 90^\circ$ means the equator is on. The transit can occur in two different ways:

1. Grazing transit $a \cos i \leq R_\star + R_H$
2. Full transit $a \cos i \leq R_\star - R_H$

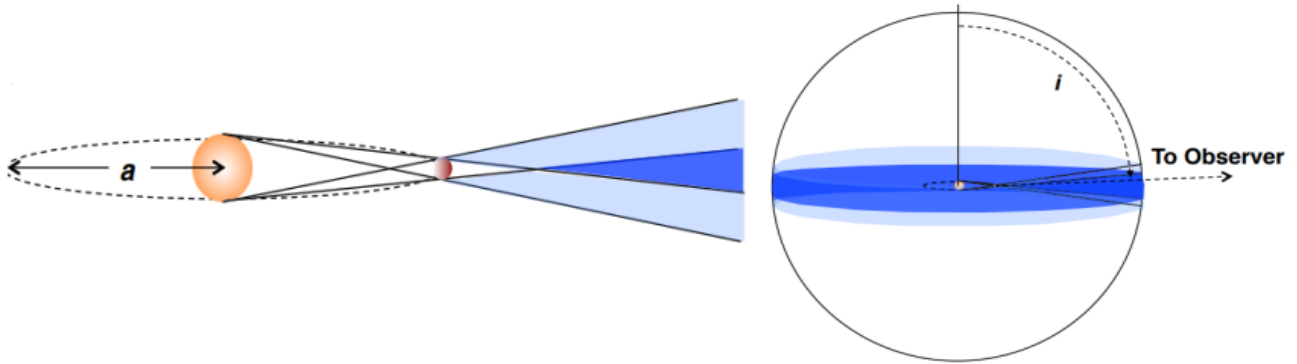


Figure 2: Something!

This is mainly dominated by the orbital inclination of the planet. Considering that the angle between the orbital inclination pole and the line of sight lies in a range $(i, i + \Delta i)$, and it is randomly distributed as was assumed before, and also that transits occur only in nearly edge-on orbits i.e. $a \cos i \leq R_\star + R_H$, we expect the probability to be uniform in $\cos i$ as shown in [Figure 3](#). Thus, the transit probability will be given by

$$P\left(\cos i < \frac{R_\star + R_H}{a}\right) = \frac{R_\star + R_H}{a} \quad (2.21)$$

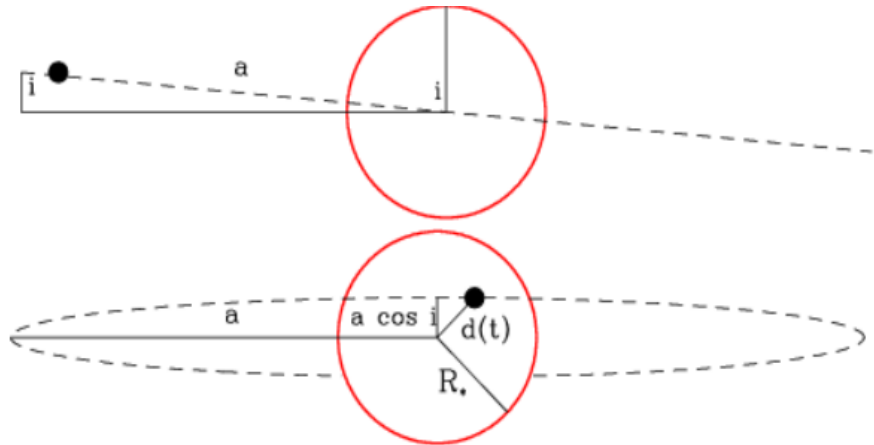


Figure 3: Something!

Then, in short, the transit probability of exoplanetary-rings in orbit around a given star where the orbital inclination is randomly distributed will be set by [Equation 2.21](#), where we only need to consider the stellar and planet Hill sphere radii R_\star and R_H respectively, and the orbital semi-major axis. Apart from this, we need to care about when, and how long the rings can co-exist inside the Hill sphere of the planet. This probability was added at the end in order to study the overall change of what was assumed in [Equation 2.14](#) and is presented in the next sub-section.

2.5.2 Rings Lifetime

It is well-known that the rings formation is a non-static phenomena, and there is no privileged epoch in the formation of a planetary system when these features can form. On the other hand the only example, so far, we have to compare with, is our own solar system, making the statistical comparison quite hard in terms of deriving the exact formation conditions and time ranges. Nevertheless, simulations and current observations allow us to estimate the main processes that modify these structures, and give us a glimpse on their formation timescales.

Currently, most of the statistics are based on *Hot Jupiters* Tiscareno,2013. However, there exists different problems with this, because the formation of rings around such objects can be affected by the low-obliquities causing the rings to edge-on or the small Hill sphere radius where they can be embedded in. In addition, viscous and Poynting-Robertson drags cause particle loss , and the high equilibrium black-body temperatures avoid materials to remain the solid state. Survival of the remnant ring depends on if they were created by tidal disruptions or continuous feeding because this will set the timescale on which the rings are expected to exist Harris,1984. In our particular case, the most important question regarding the rings is: What is their age?. This is because we need to know how long they are expected to live in order to properly compute the probability of observing ring systems around a planet given the overall age of the star and the planetary system itself. The age of the rings can be affected by the mean residence time of the particles on the rings or by how long the structure/sources have been in place For example in the case of Jupiter, if some moons suddenly disappear, or cease emitting dust, the rings will dissipate in $\sim 10^5$ yr Tiscareno,2013. Interaction and physical processes may change or reset the age as can be the shepherding of the moons inside the rings leading to an age range of 100×10^6 - 6×10^8 yr Colwell,1994, or ring's viscous spreading (10^5 - 10^9 yr based on Saturn's ring A) Charnoz et al.,2009 or ($\sim 10^9$ yr) from viscous timescales if the gas is considered to be non-turbulent Harris,1984. There exists also the chance that the ring is completely disrupted (based on the fragmentation criteria), so in that case we end up with a time for complete loss of the rings of 10^7 - 10^8 yr Colwell,1994 or based on evolutionary processes $< 10^8$ yr Charnoz et al.,2009. On the other hand, considering cometary passages which could break a satellite or to tidally disrupt the comet applied to Saturn's ring lead to a time range of 10^7 - 10^8 yr for the A-ring, 10^8 - 10^9 yr for the B-ring, and 10^7 yr from radial spreading Charnoz et al.,2009.

As has been presented above, different age ranges can be derived for the rings lifetime through models and observations of our own solar system. However, the remaining question is: Do they form at the very beginning, the middle or the end of the planetary system formation?. According to Charnoz et al.,2009 the main core of Saturn's B-ring was formed in the first Gyr of the solar system in which collisions are expected to be much more likely. However, from simulations it is pointed out Saturn's ring formation can be understood a huge disruption near the end of the planetary formation period during which the circum-planetary gas disk is still present Canup,2010. If we look to Uranus or Neptune, possibly they have been less affected and have not changed dramatically over the age of the solar system, where rings and moons has been oscillating between accretion and disruption for many Gyr Tiscareno,2013.

In general, there is no complete consensus on whether the rings form at the beginning, or at the end of the planetary formation process, neither on the time they can live as a ring-structure around the planet. Base don this, we decided to introduce a fifth probability to account for the

most likely lifespan a ring can have. The probability is defined in [Equation 2.22](#), but it is necessary to have in mind that as it is hard to guarantee the exact moment in time where they form, then this probability assumes each time interval has the same chance and we can only provide an estimation based on the mean-rings lifespan and the stellar age.

$$P_5 = \frac{\text{Rings lifespan}}{\text{Host star's age}} \quad (2.22)$$

2.6 MONTE-CARLO SIMULATIONS

As was shown in [Section 2.2](#), we have two different ways to generate the exoplanetary mass-period distribution either by considering a weak correlation i.e. β -distribution or using a simple power law derived from the observations. One way or another, we are able to generate a new sample of planets with mass and period following a given distribution using the Monte-Carlo method. This method consists in drawing a sample of N values which follows the wanted distribution using randomly distributed numbers.

In the first case, we have the β -distribution addressed in [Section 2.3.1](#). A sample of 10.000 mass-period pairs were generated following [Equation 2.23](#), where (α_m, β_m) , (α_p, β_p) , and (δ_1, δ_2) were created using pseudo-random numbers following a β -distribution as pointed out in [Jiang et al.,2007](#). The mass and period range covers $0.008 \leq m/M_j \leq 26.7$, and $0.8079 \leq p/\text{days} \leq 6776.1$ respectively.

$$\begin{aligned} m &= 155.5 * (\alpha_m + \delta_1) / (\alpha_m + \delta_1 + \beta_m + \delta_2) \\ p &= 11650.0 * (\alpha_p + \delta_1) / (\alpha_p + \delta_1 + \beta_p + \delta_2) \end{aligned} \quad (2.23)$$

The period/mass, period/semi-major axis, and mass/semi-major axis are shown in figures [Figure 4](#),[Figure 5](#), and [Figure 6](#) respectively where each dot corresponds to each pair generated using the β -distribution method, and the semi-major axis was computed using Kepler's third law.

On the other hand, we decided to use the single power law approach as suggested by ([Cumming et al.,2008](#); [Butler et al.,2006](#)) to generate the mass-period distribution for exoplanets, and also following the well-known Slapeter- and-Kroups's power law to generate the stellar masses as was explained in [Section 2.4.1](#) and [Section 2.4.2](#) individually. Following this method, we set the values for the exponents in the case of the exoplanets to 1.16 and 0.74 for the mass and the period respectively as suggested in [Nielsen et al.,2010](#) who basically based his results on different observations and corrections to values previously obtained by [Cumming et al.,2008](#) and [Butler et al.,2006](#)). According to the last, we can generate a sample of exoplanetary masses and periods in a range covering $0.3 \leq m/M_j \leq 10$, and $2 \leq p/\text{days} \leq 2000$. This a slightly smaller range compared to what the β -distribution method can provide but it is still useful because it lies in the range we are interested in. Thus, a sample of 10.000 pairs was drawn following the method

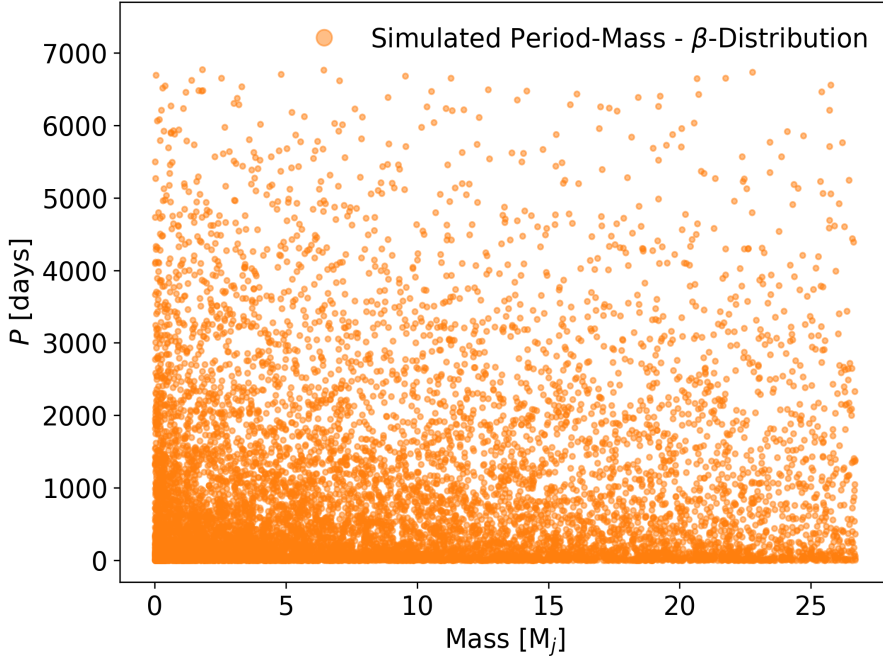


Figure 4: Something!

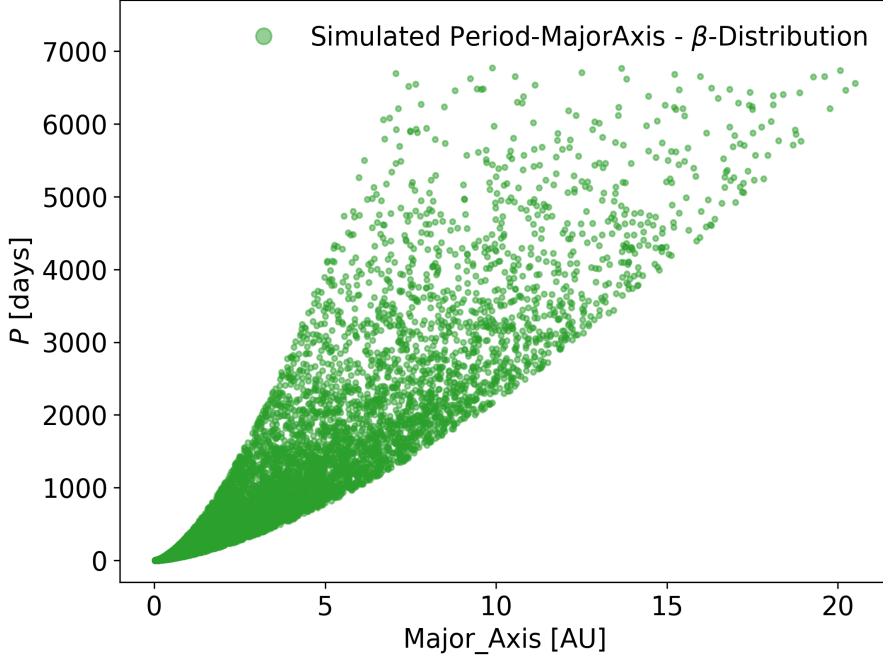


Figure 5: Something!

explained in [Section 2.2](#). In [Figure 7](#) and [Figure 8](#) the histogram and the cumulative function for the generated values are shown in blue whilst the orange dashed line shows the expected shape that these values should follow from the original power law. The figures on the left are shown in linear scale while those on the right are in logarithmic scale. As can be seen, both the mass and period values simulated follow the original power law. For comparison as in the last case, the period/mass, period/semi-major axis, and mass/semi-major axis are shown in figures

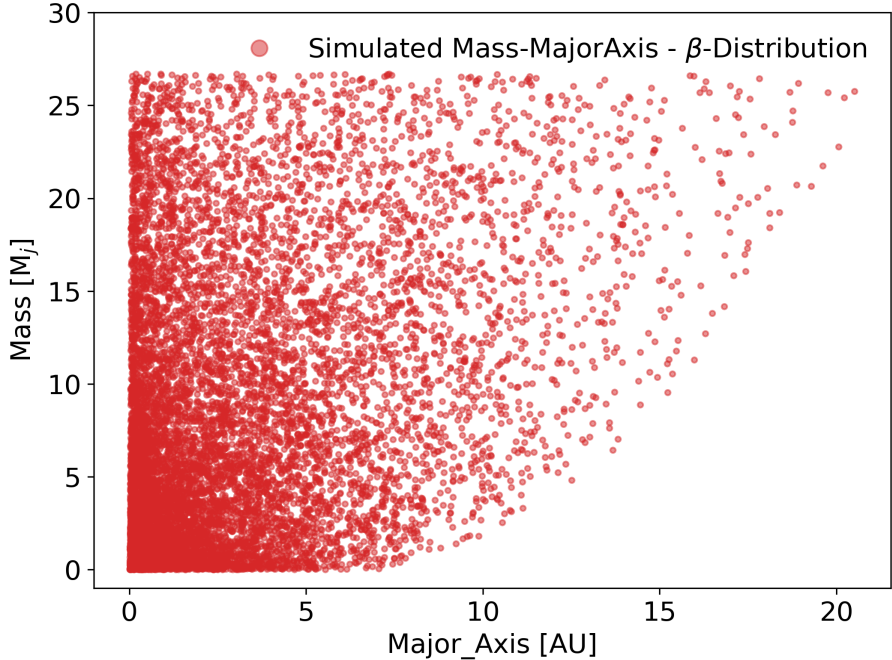


Figure 6: Something!

[Figure 9](#), [Figure 10](#), and [Figure 11](#) respectively. In both cases, the β -distribution and the power-law method reproduce the observed distribution of mass and period, however, as using the power law we can double check that the simulated values follow the original trend, which is not the case for the β -distribution where the constants are imposed from their observations, we will use the power-law method to generate our final sample of mass-period pairs.

Finally, the same power-law method was used to generate the stellar mass. As was introduced in [Section 2.4.1](#) and [Section 2.4.2](#), we have two different power laws which can describe the stellar mass functions. Taking into account that in general there is no consensus on a single exponent which could describe the distribution of stellar masses in the universe, we decided to test both exponents but paying more attention to the Kroupa's initial mass function distribution due to the fact that gives different values of the exponent to small masses which is the actual problem in astrophysics. Following this, we created once again a sample of 10.000 stars following the initial mass function described by a Salpeter's and Kroupa's exponent. In the case of Salpeter, the mass range covers $0.1 \leq m/M_{\odot} \leq 10$ with an exponent of 2.35, whilst the Kroupa's range covers $0.1 \leq m/M_{\odot} \leq 0.5$ with an exponent of 1.3, and an exponent of 2.3 for $0.5 \leq m/M_{\odot} \leq 10$. The drawn distributions are shown in [Figure 12](#) and [Figure 13](#), where the histogram and cumulative functions are shown in blue and the original power law distributions are shown with the dashed orange line. In the case of the Kroupa's distribution, a fine break can be seen in the logarithmic scale figure for the small stellar masses due to the fact that we are using two different exponents for different mass ranges.

Summarizing, we generated a sample of 10.000 exoplanetary mass-period pairs and stellar masses individually following in the case of the exoplanets β -distribution or a simple power law, and in the case of the stellar initial mass function using two different power laws known as Salpeter's and Kroupa's initial mass function. As we different ways to generate mock samples,

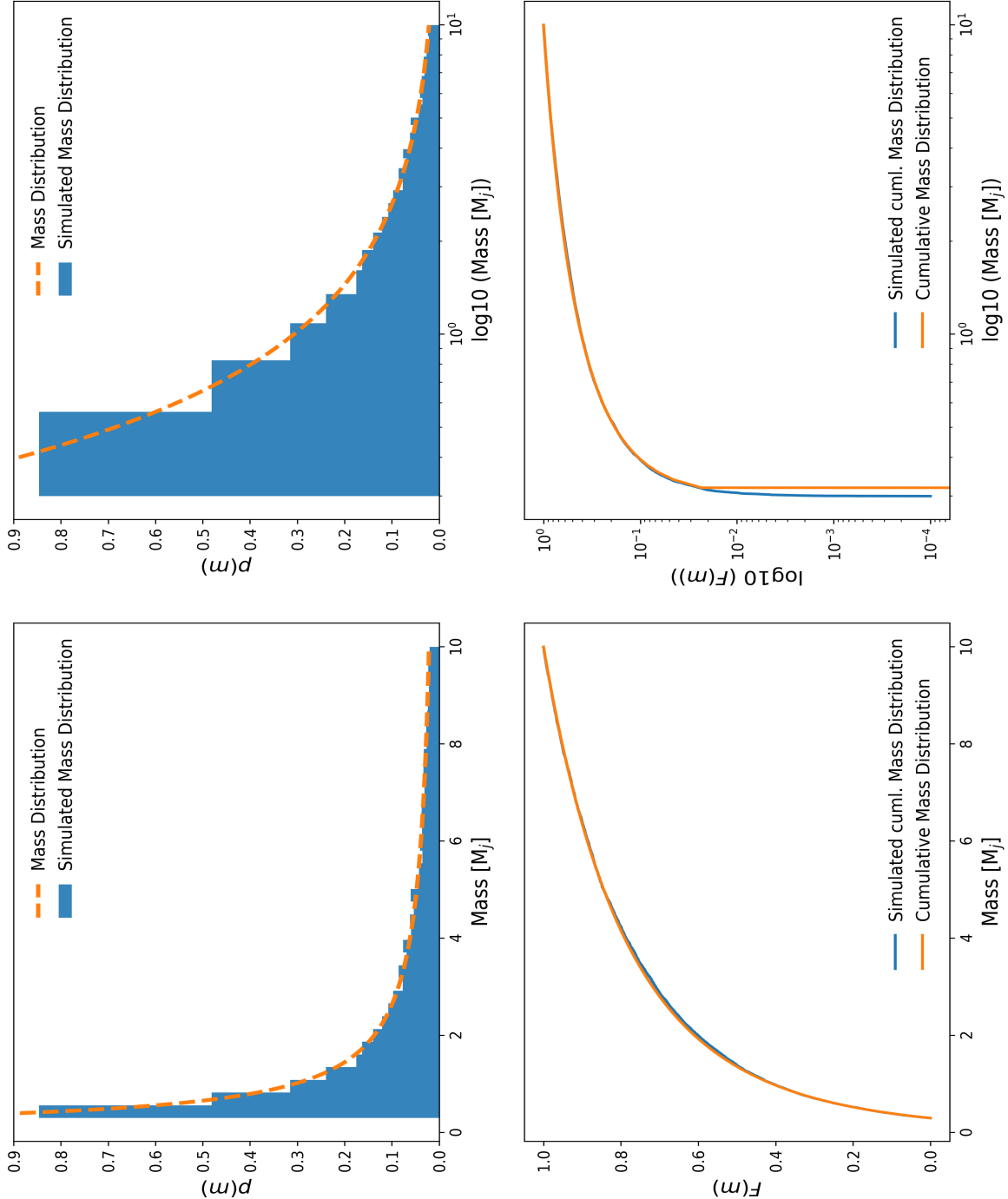


Figure 7: Something!

we decided to stick to the power law generation in the case of the exoplanetary mass-period distribution because we are able to check the cumulative function and if the actual drawn pairs follow the original distributions. In the same way, for the stellar mass generation we decided to use the Kroupa's distribution because it treats in a different fashion i.e. different power law value, the small masses which are really important in the scenario we are considering. Having said this, we proceed to use these values and the previous information presented in the last sections to compute the probability of transit detection. This is thoroughly explained in [Section 2.7](#) in which

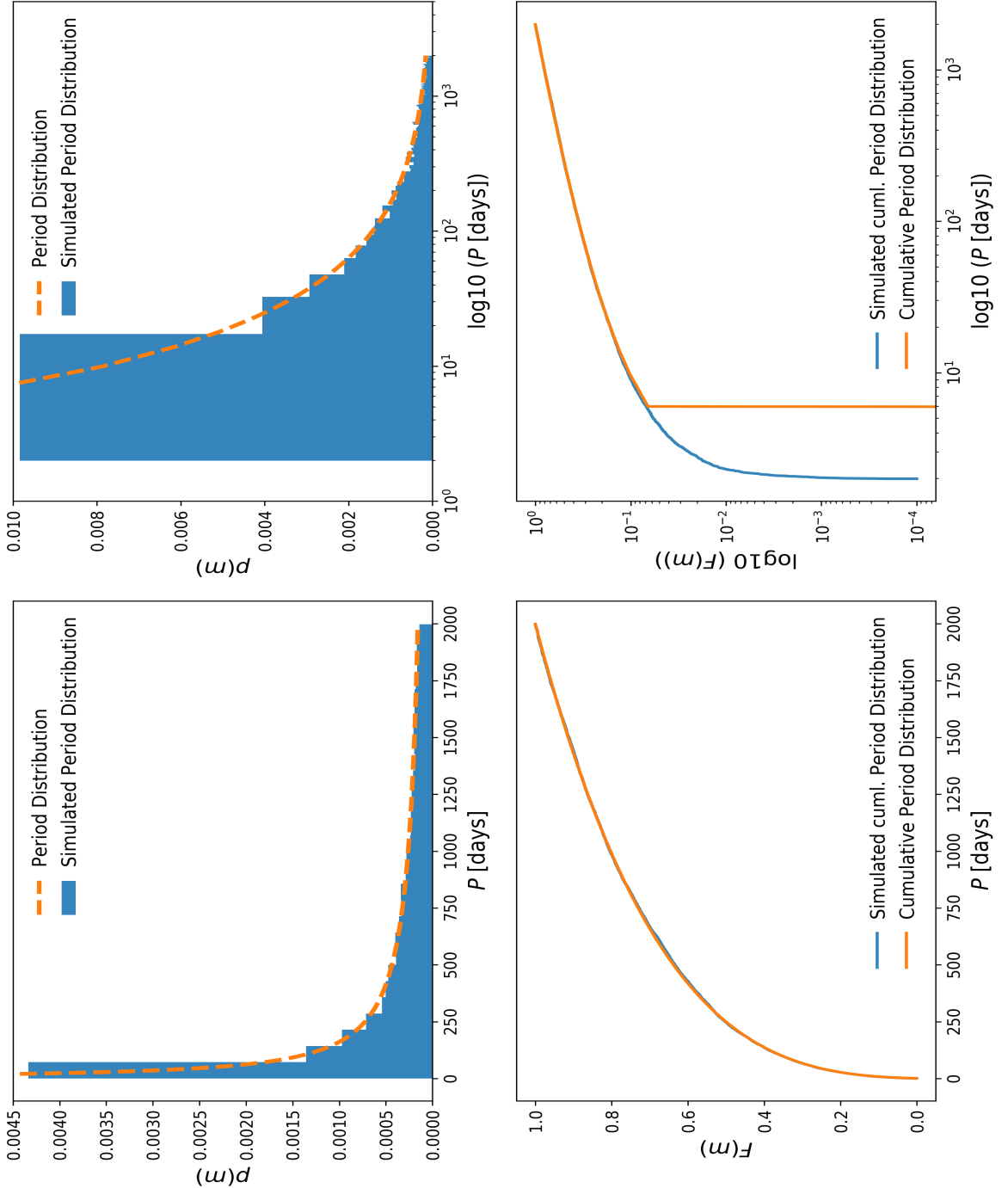


Figure 8: Something!

we address this calculation in two different ways. Firstly, using the results from the Monte-Carlo simulations, and secondly evaluating directly the analytic form of the transit probability.

2.7 DETECTION PROBABILITY: MONTE-CARLO VS ANALYTIC FORM

In Section 2.5, the main components of the probability of a ringed-system transiting in front of its parent star was addressed. However, the main goal is to constrain for the different exoplanetary

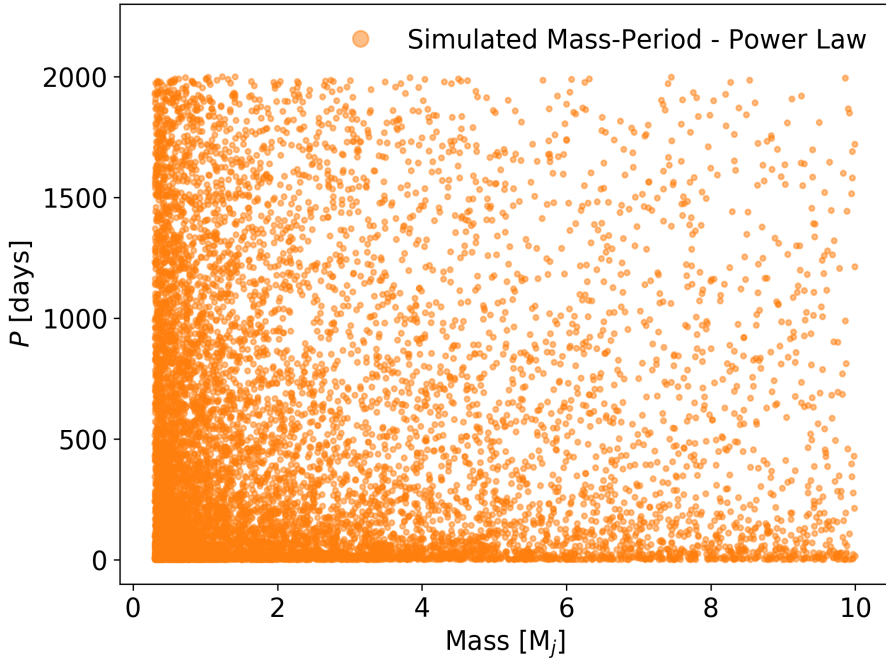


Figure 9: Something!

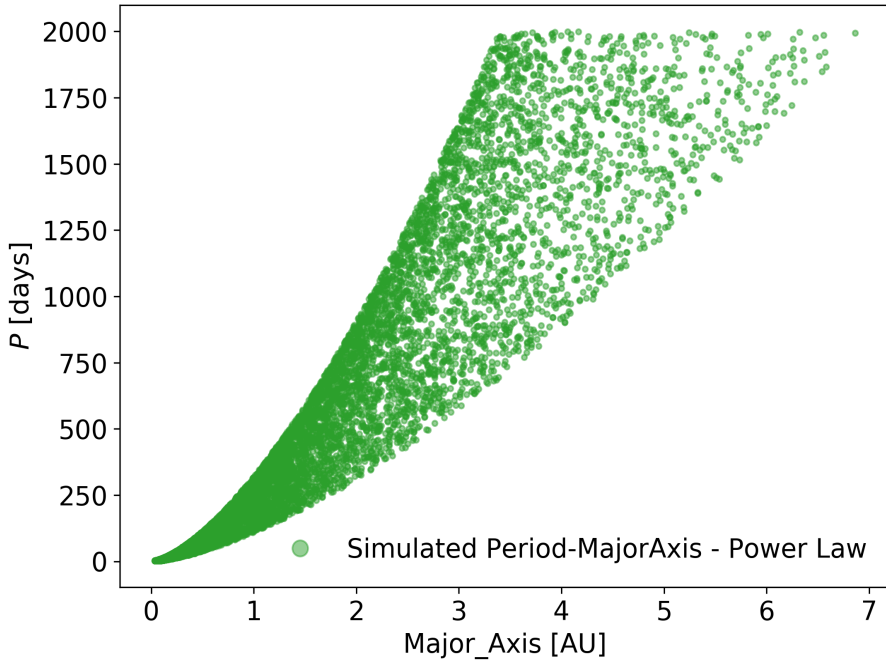


Figure 10: Something!

mass-period pairs how it changes as a function of the stellar mass. We decided to tackle down this problem in two different ways: i) using the Monte-Carlo results for the exoplanetary mass-period distributions, and ii) simply generating the probability from the analytic form without recurring to any Monte-Carlo generation of values. In both cases, we use the probability function shown in [Equation 2.24](#) which does not include the fifth probability corresponding to the planetary rings'

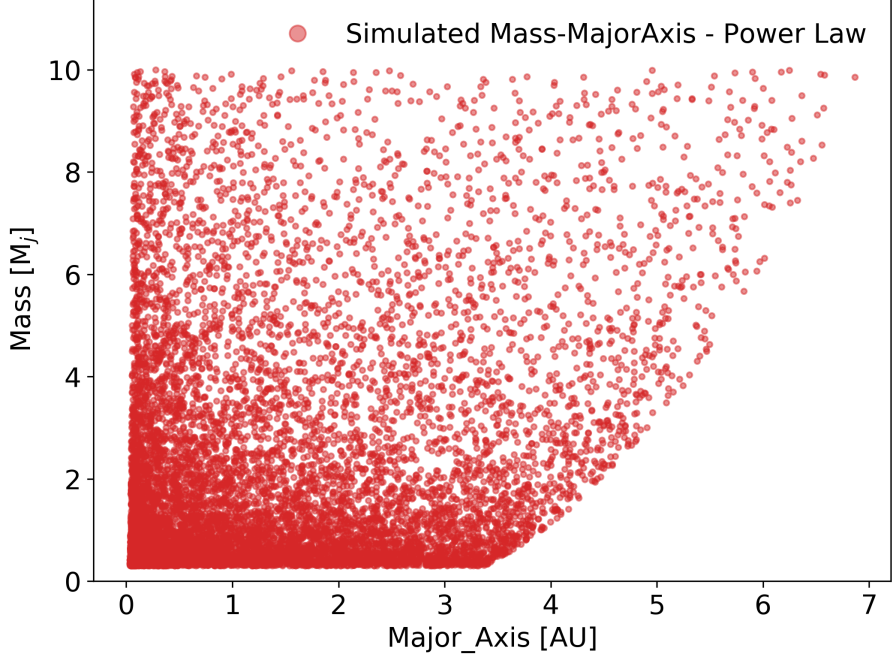


Figure 11: Something!

lifetime. this will be addressed separately at the end of this section.

First of all, in the case of the Monte-Carlo process, a sample of 10.000 stars between $0.1 \leq m/M_{\odot} \leq 10.0$ was generating following the Kroupa's initial mass function. Moreover, a sample of 10.000 mass-period pairs were also generated following the power law distribution suggested by Nielsen et al., 2010 and explained in Section 2.6. Once we have set the final sample of exoplanets and stars to be tested, we proceed to evaluate out the detection probability function which is given by Equation 2.24. It is important to have in mind that in this equation the values corresponding to the exoplanetary mass and period are taken from the Monte-Carlo simulation. Also, the semi-major axis is obtained using Kepler's third law, and the stellar mass is obtained with the Monte-Carlo generation as well. We need to have a relation between the stellar masses and stellar radii. To achieve this goal, we used two different approaches. The first one assumes that the stars are in the main sequence and follow the regular relation given by $R \propto M^{0.8}$, however this assumes that the stars are already in the ZAMS, have the solar metallicity and are massive stars burning H to He via the CNO chain. This not entirely true for our purposes because we aim to study young stellar populations. Thus, we decided to use the *MESA*-code provided through the *MIST*-package (Dotter, 2016; Choi et al., 2016) to compute the stellar isochrone for a 20Myr star varying the masses between $0.1 \leq m/M_{\odot} \leq 10.0$ which is the range we are interested in. In Figure 14, the stellar radius versus the stellar mass obtained using the 20Myr isochrone is shown. The blue dots correspond to the values retrieved by the model while the orange dots represent a linear interpolation performed to complete some empty regions in the isochrone. Once this is settle, we can assign the expected stellar radius for a given mass assuming that the stellar age is

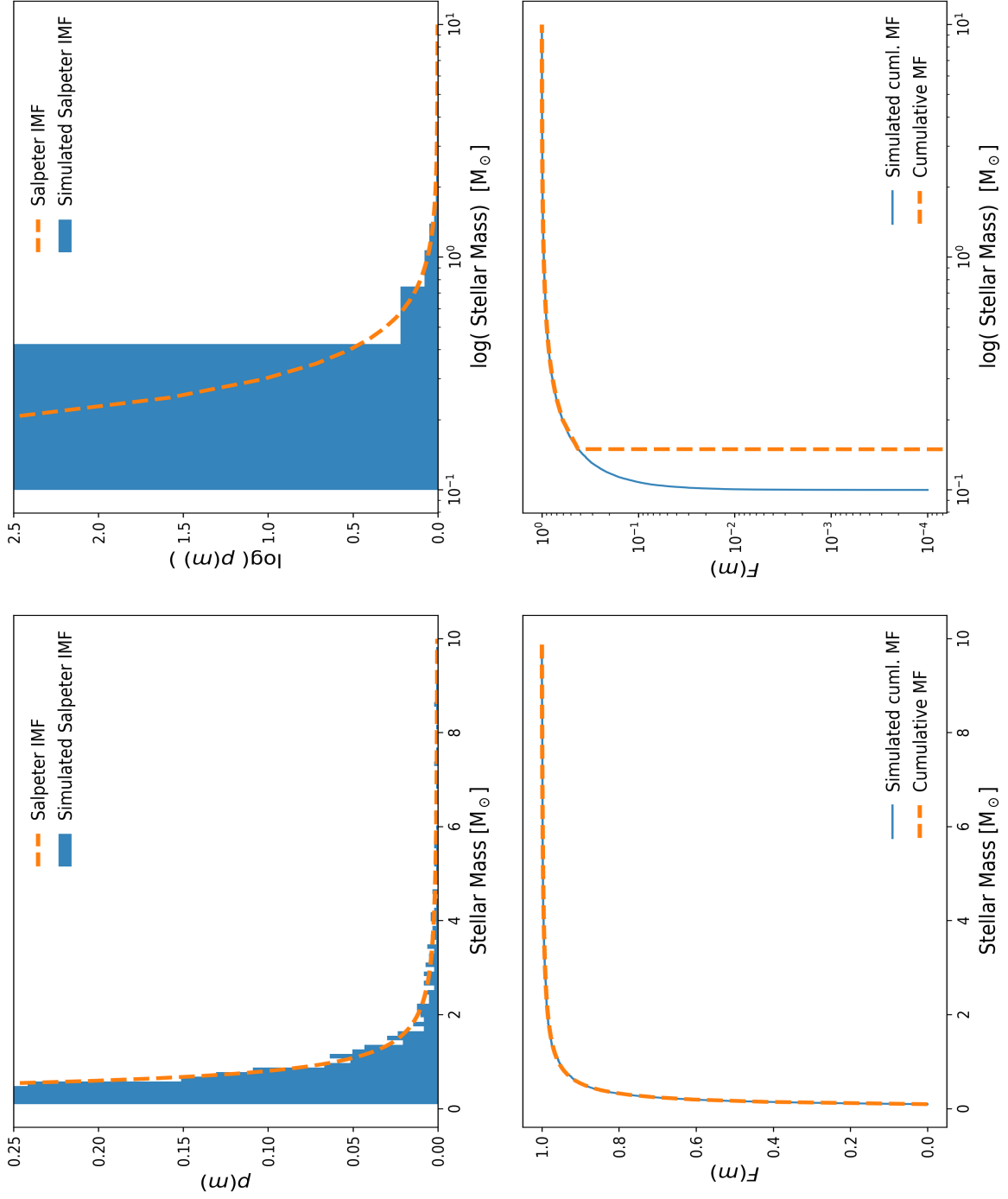


Figure 12: Something!

close to $20M\text{yr}$.

$$\text{Detection Probability} = 0.17 \left(\frac{R_\star + R_H}{a} \right) \left[1 - \left(\frac{\text{Gaia Duration} - \text{Eclipse Duration}}{\text{Gaia Duration}} \right)^n \right] \quad (2.24)$$

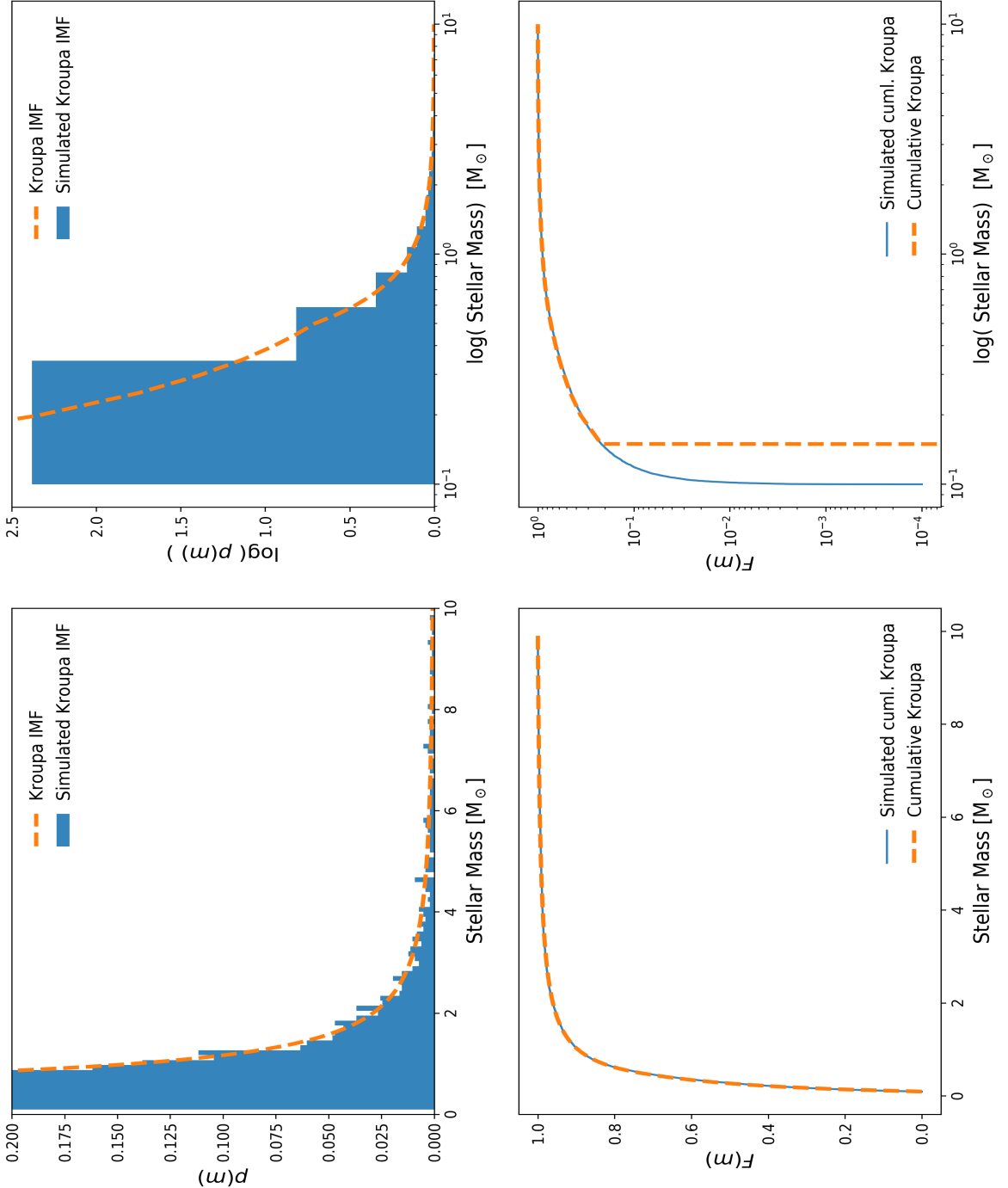


Figure 13: Something!

Once the function is evaluated using all the different parameters described above, we end up with a detection probability distribution for each exoplanet as a function of the stellar mass as shown in [Figure 15](#). Panel (a) shows the detection probability as a function of stellar mass computed through [Equation 2.24](#) for five random selected values out of the 10.000 simulated. Panel (b) shows exactly the same parameters but in this case the detection probability was summed up

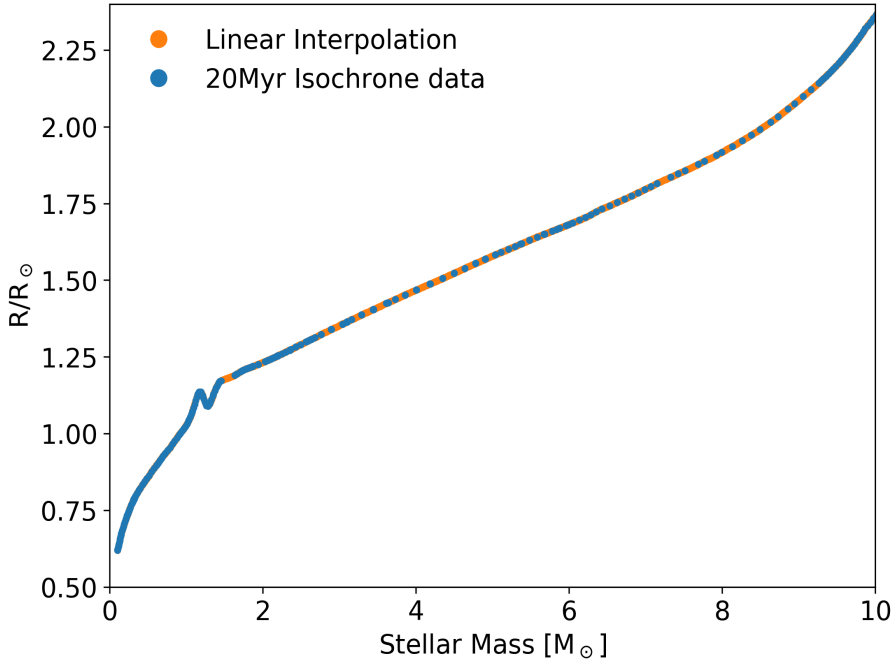
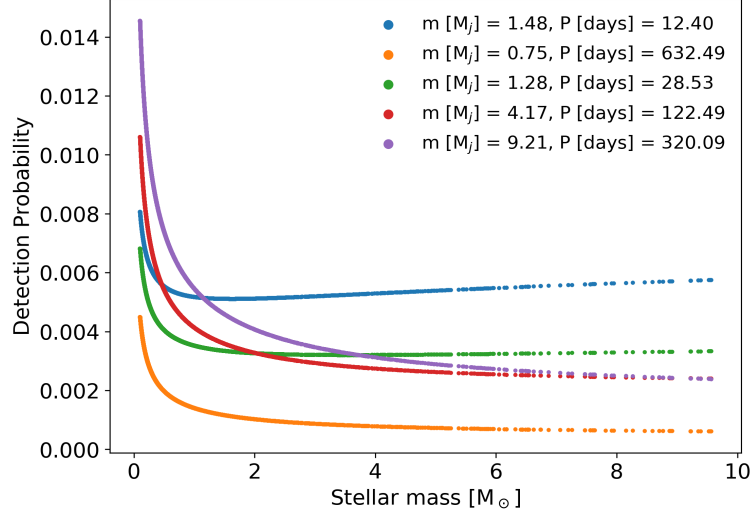


Figure 14: Something!

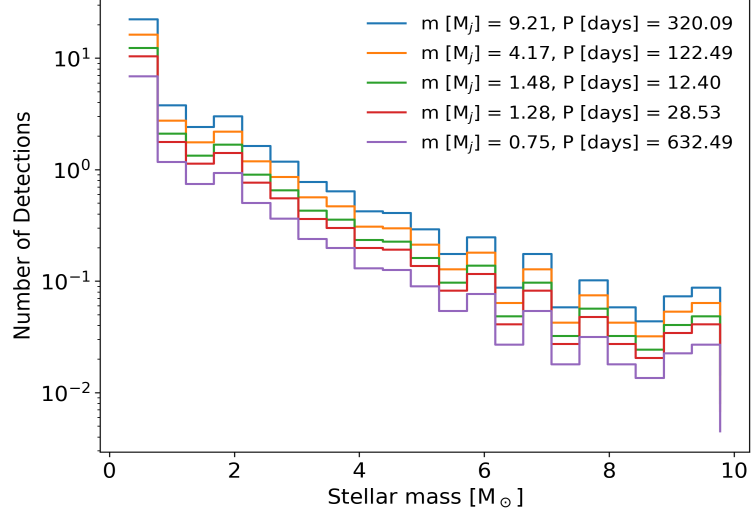
in bins of $0.5M_{\odot}$ to obtain the number of detections expected.

On the other hand, we evaluated directly [Equation 2.24](#) where instead of summing up each value inside a given bin, we integrate this function and use a weight to re-scale the values using the fact that as the stellar initial mass function follows a power law, it is possible to integrate each mass bin between boundaries m_1 and m_2 while leaving the total number of stars fixed i.e. $N = 10.000$, and finding the proportionality constant. This way it is easy to compute the number of detections without recurring to a generation of large samples using the Monte-Carlo approach. To check this, we decided to test an exoplanet of $10M_{\oplus}$ and 5yr period. First, using the Monte-Carlo process to generate the 10.000 starts following the Kroupa distribution and evaluating [Equation 2.24](#) with fixed exoplanetary mass-period. After this, the detection probability was summed up in bins of $0.5M_{\odot}$ and the result is shown in [Figure 16](#). However, for the second case, [Equation 2.24](#) was directly evaluated in regular stellar mass array without any Monte-Carlo approach, and the detection probability was integrated fixing the total number of stars to re-scale each bin. The final result is shown in [Figure 17](#). As can be seen from [Figure 16](#) and [Figure 17](#) both approaches lead to similar results, although in the case of the analytic form the slope is a bit steeper due to the fact that we are considering a fixed number of stars per bin derived from the continuity equation from the power law as explained before. If we reproduce the Monte-Carlo process several times we will eventually end up in this case. In brief, the analytic form approach will be used to study the dependence of this detection probability and the number of expected detections as a function of the fifth probability which was not introduced here and it is related to the lifetime of the planetary rings.

It was pointed out in [Section 2.5.2](#) that there is no general consensus on the timescale in which planetary rings are created or for how long they survive. However, based on our own solar system there is a range of possible values which will give a glimpse on this value. We decided to test how



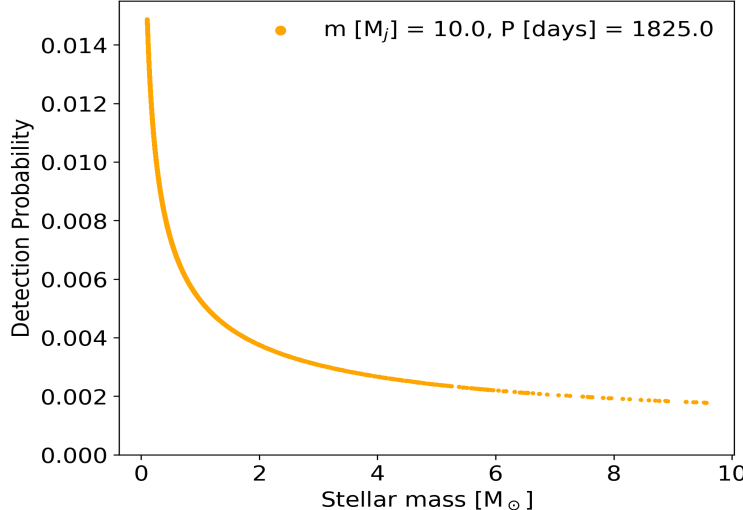
(a) label 1



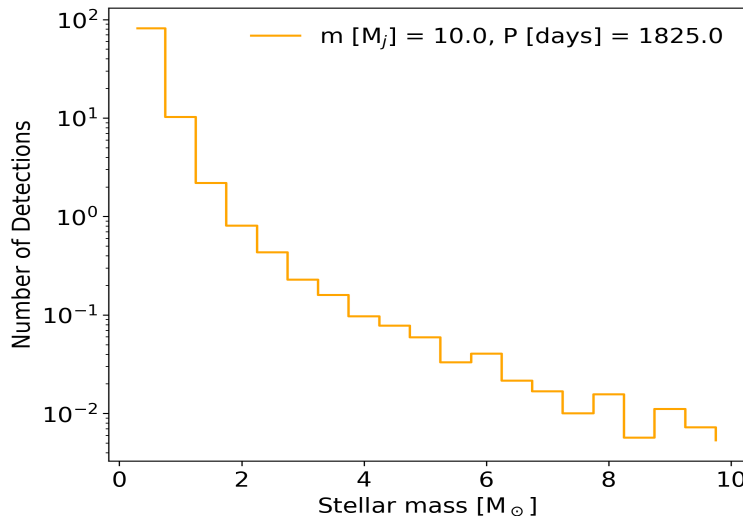
(b) label 2

Figure 15: Something!

the detection probability and the number of detections change for different values. In [Figure 18](#) each line was computed using the last method, avoiding the Monte-Carlo calculation for different rings' lifetime spanning from 1×10^5 yr to 1×10^7 yr because it was the most reliable range of values found in literature. The case in which the rings are not taken into account corresponds to the 0.0 yr value. It is clear that the younger the exoplanetary rings, the lower the probability of detecting them around the stellar system because as was shown in [Equation 2.22](#) this probability is computed as a ratio between the the rings' lifetime and the stellar age. Thus, the larger the timescale, the larger the probability, and so the detections. This is really important because depending on this value we can expect different number of transits in a certain stellar mass range. However, it is worth noting that the highest probability is achieved towards the small stellar mass values.



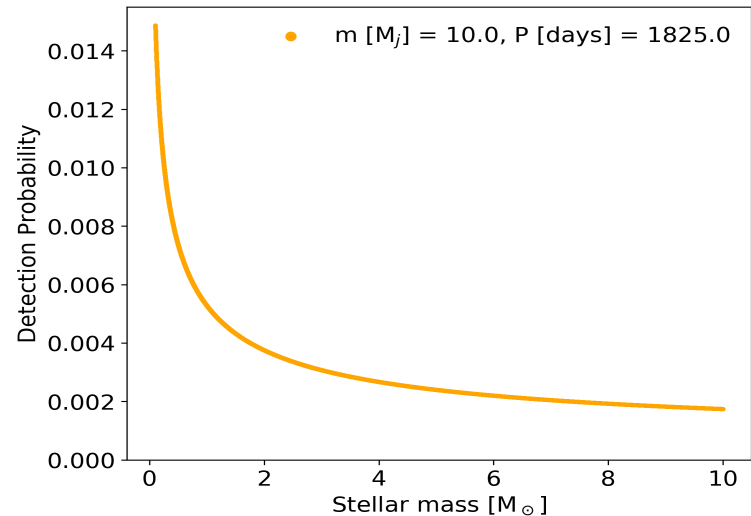
(a) label 1



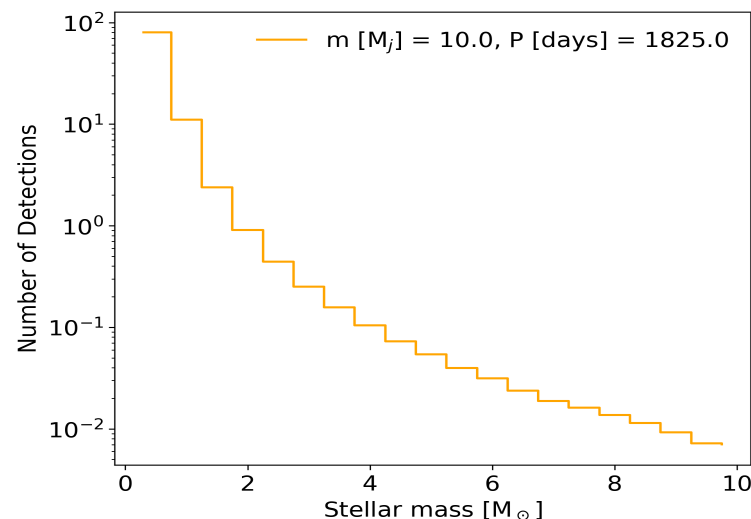
(b) label 2

Figure 16: Something!

In conclusion, we present different ways to calculate the expected number of detections. However, we decided to stick to the analytic form instead of using the Monte-Carlo process just for simplicity though both methods lead to the same results in overall. Also, there are different ways to generate the stellar masses named the Salpeter or Kroupa's initial mass functions. All the methods explained above are available in the Git-Hub repository <https://github.com/Jurgenvilla/Exoplanet-Rings-and-Gaia>. It is however worth noting that the main conclusion from this analysis relies on the fact that the number of planetary detections increases for the low-mass stars. This is really important in our work as we want to focus on young stellar populations which are mainly composed of proto-stars which are accreting gas and are still forming. It is expected to test this assumptions and how reliable each probability involved in this process is with actual observations.



(a) label 1



(b) label 2

Figure 17: Something!

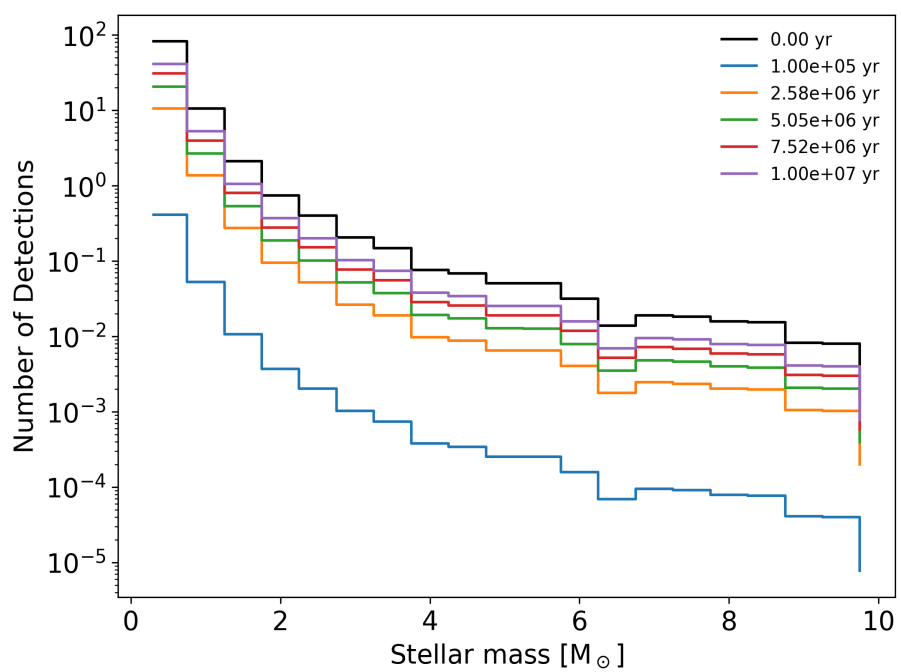


Figure 18: Something!

GAIA AND SUPERWASP SAMPLE DATA

3.1 INTRODUCTION

The main goal of the project is to target young-star populations to enhance the probability of observing exoplanetary rings transiting in front of their parent star. Therefore, we mainly focused our study in the well-known OB association Sco-Cen which is mainly sub-divided into three different regions: Lower Centaurus Crux (LCC), Upper Centaurus Lupus (UCL), and Upper Scorpius (US). The *Gaia*-DR1 and-DR2 data were used to select the final sample of stars satisfying conditions on the distance, parallaxes and proper motions based on previous research (Wright and Mamajek,2018; Pecaut and Mamajek,2016; de Geus et al.,1989). However, also a selection based on stellar evolution tracks and isochrones using the *MESA*-code provided through the *MIST*-package (Dotter,2016; Choi et al.,2016) was performed to guarantee that the final sample consists of stars between 5Myr to 60Myr. This informations is needed in order to obtain the *RA* and *DEC* coordinates of the objects of interest and retrieve the available light curves using the *SuperWASP*-database (Butters et al.,2010). The main results from the *Gaia*-and *SuperWASP*-queries are presented in more detail the next sections, including the light-curves preliminary results which are addressed extensively in Chapter 4 .

3.2 SCO-CEN OB ASSOCIATION

3.3 GAIA SAMPLES

The *Gaia*-DR1 and-DR2 data was used to select stars which belong to the Sco-Cen OB association. The queries were carried out using the ADQL-query interface provided by the ESA (<https://gea.esac.esa.int/archive/>) and shown in Chapter 6 for each of the three regions conforming Sco-Cen i.e. LCC, UCL, and US. The approach was tested in *Gaia*-DR1, but later on was extended to the new data provided by the DR2 to increase the sample of stars belonging to Sco-Cen, and also to increase the chance of matching a star with a light curve in the *SuperWASP*-database. This will be addressed at the end. The most relevant parameters retrieved for each object are the RA and DEC coordinates, galactic longitude (l) and latitude (b), parallax, magnitude in the G-band, color G-Ks, and the proper motion in RA and DEC.

First of all, a sample based on previous physical parameters and values obtained for this association is needed in order to constrain the sample and avoid pollution from stars which may not be part of it. Following Wright and Mamajek,2018, the spatial distribution of the three regions were selected using the galactic coordinates cut reported by Rizzuto et al.,2012 and de Zeeuw et al.,1999 as shown in Table 1. Also in distance, using a parallax range from 6mas to 12mas which leads to a distance range of $\sim 83 - 167$ pc. We decided to include a wide range in distance because Sco-Cen spanning distances are known to be $\sim 100 - 150$ pc Wright and Mamajek,2018, so we can rule out any outliers based on the dynamics of the cluster. The spatial distribution

Table 1: Something!

Sub-group	l_- [deg]	l_+ [deg]	b_- [deg]	b_+ [deg]
Lower Centaurus Crux	285	313	-10	16
Upper Centaurus Lupus	313	337	5	31
Upper Scorpius	337	360	7	32

of our sample is shown in [Figure 20](#). The blue, orange, and red dots represent LCC, UCL, and US respectively. It is clear that the Sco-Cen association covers a wide range in galactic longitude (l) ~ 90 -deg, and ~ 45 -deg in galactic latitude (b). Following this, initially each sub-region contains LCC = 2310, UCL = 1759, and US = 1584 stars respectively. However, as it is mentioned in [Pecaut and Mamajek, 2016](#), each region has a characteristic range for the proper motions given by the dynamics of each individual subgroup and the whole interaction. According to their work, the three subgroups have a value of $\mu_\alpha < 10 \text{ mas yr}^{-1}$ and $\mu_\delta = 30 \text{ mas yr}^{-1}$, while for LCC, UCL, and US values of $15 \text{ mas yr}^{-1} < \mu < 55 \text{ mas yr}^{-1}$, $12 \text{ mas yr}^{-1} < \mu < 55 \text{ mas yr}^{-1}$, and $\mu < 47 \text{ mas yr}^{-1}$, respectively, are reported. This is better seen in [Figure 19](#) where the histogram for the whole sample of stars selected in distance range are shown in colors, and each vertical dashed-line shows the above mentioned cuts for each subgroup. In the end, after this analysis, the query was performed taking into account the dynamical constraints of the cluster (see [Chapter 6](#)).

This cut-off in proper motion and parallax leads to a new sample of LCC = 1010, UCL = 746, and US = 797 stars respectively, in which we have ruled out stars which certainly do not belong to the association. The next step is to narrow down the sample based on the stellar evolution of the cluster. This was performed using evolutionary tracks in which we aimed to use low mass stars as they are the ones with higher probabilities of exo-ring transits as shown before, and also using isochrones to restrict each sample in stellar age. This is thoroughly explained in [Section 3.4](#).

3.4 STELLAR EVOLUTION MODELS

The highest transit probability was obtained for low mass stars. As shown in [Figure 18](#), the probability of detecting rings transiting in front of the parent stars decreases as the stellar mass increases independent of the life time for the planetary rings which only causes a vertical shift i.e. a chance in the expected number of transits. Therefore, it is important to select a reliable sample of stars in Sco-Cen which can lead to a high chance of detecting this kind of transits. The first step consisted in taking the sample mentioned above in which a cut-off in the dynamics and distance for the association has been applied, and run different stellar track models with an initial value of extinction $A_V = 0$ for each sub-region using the *MIST*-package. In [Figure 21](#), the color-magnitude diagram for each sub-region is presented for G- and K_s-bands. The magnitudes were obtained using *Gaia*-DR1 and transformed to absolute magnitude (see [Chapter 6](#)). The color was computed using a cross-match identification of the sources in *Gaia*-DR1 with *The Two Micron All-Sky Survey* (2MASS) tables. The stellar tracks shown correspond to stellar masses from $0.5M_\odot$ to $2.1M_\odot$ in steps of $0.4M_\odot$, which were computed for the required photometric bands in *Gaia* and 2MASS. Although each sub-region shows different spread, the stars seem to be distributed mostly below the $1.3M_\odot$ stellar track. Therefore, no-extra cut-off in mass is needed because if one compares to [Figure 18](#) the highest probabilities lie below $2.0M_\odot$. The same

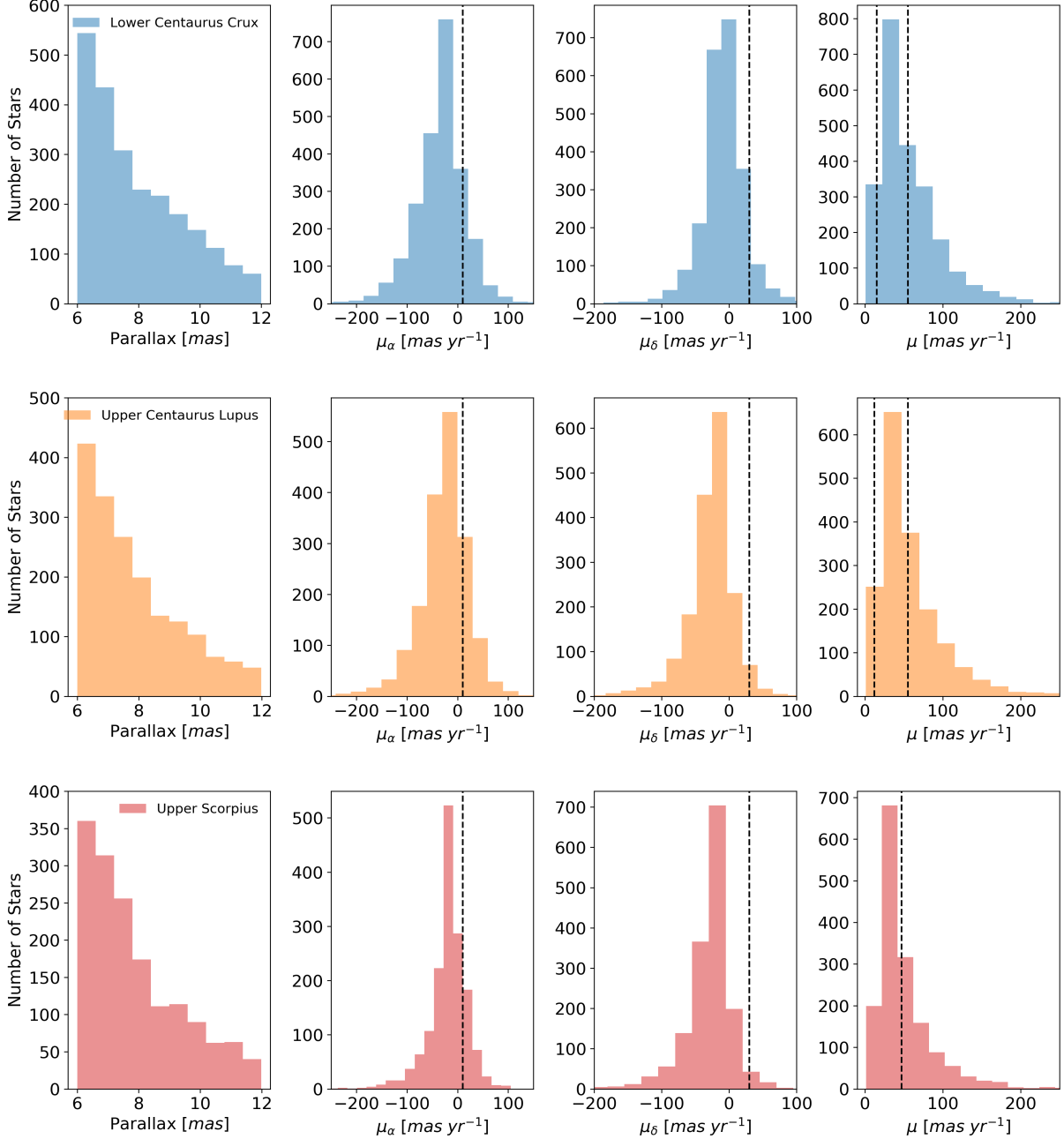


Figure 19: Something!

conditions were assumed to compute the isochrones shown in Figure 22. Each figure corresponds to the LCC, UCL, and US color-magnitude diagrams with isochrones of 5, 15, 20, 30- and 60-Myr. The upper isochrone, is the youngest (5-Myr) while the lower represents the oldest (60-Myr). In each of the three cases, most of the stars are contained in between the youngest and the oldest isochrones. It is useful to have in mind that all the isochrones are computed without extinction factor which is the ideal scenario. A few stars lie outside the isochrones delimited region, thus, the idea is to use the isochrones and only use those stars that satisfy the absolute magnitude M_G and color $G - K_s$ conditions in between both isochrones. After obtaining only those stars in between the isochrones the final sample is reduced to LCC = 868, UCL = 633, and US = 649 stars

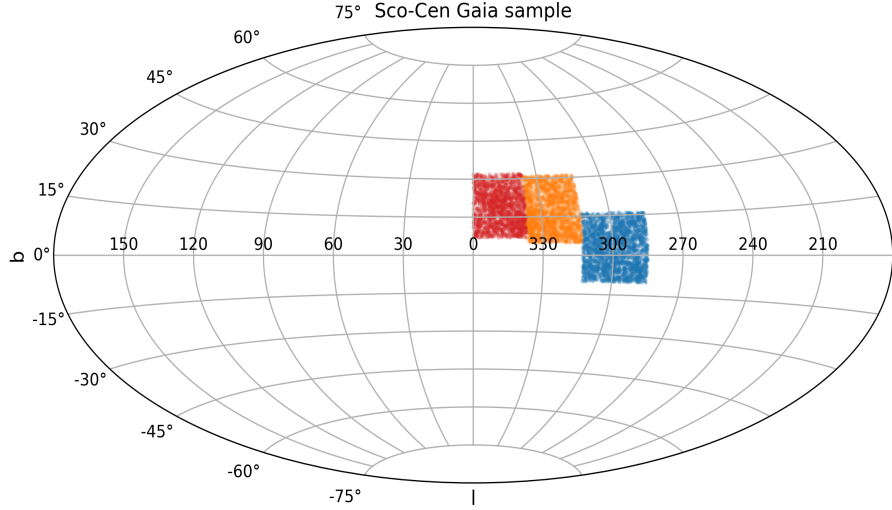


Figure 20: Something!

respectively. This is shown in [Figure 23](#) where one can observe how the initial distribution of stars is already contained in a region delimited by the isochrones. For comparison in [Chapter 6, Section 6.2](#), it is shown the original sample of stars without performing the proper motion and parallax cut-off in color versus the sample after using [Pecaut and Mamajek, 2016](#) constraints in black-dots for each sub-region in [Figure 28](#) and [Figure 29](#).

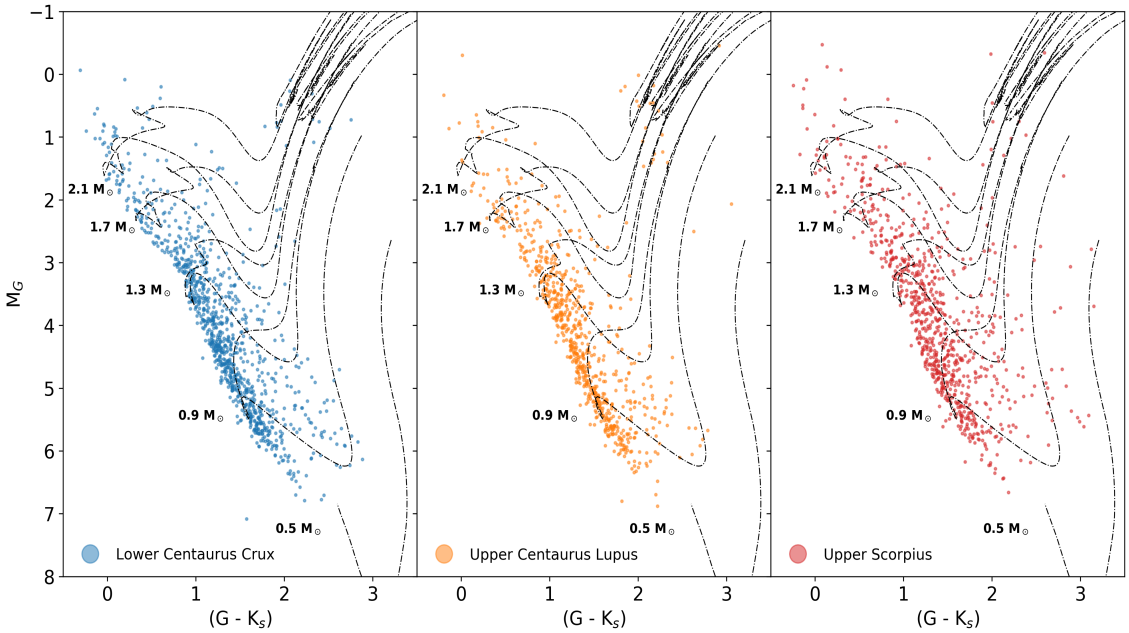


Figure 21: Something!

Besides this, if we want to obtain a reliable sample of star which belong to Sco-Cen, we need to include the extinction in each sub-region when computing the stellar tracks and isochrones. As can be seen from [Figure 22](#), the 60-Myr gently touches the main-sequence of this association, thus, it seems legit to compute this isochrone with $A_v = 0$ because extinction will shift the

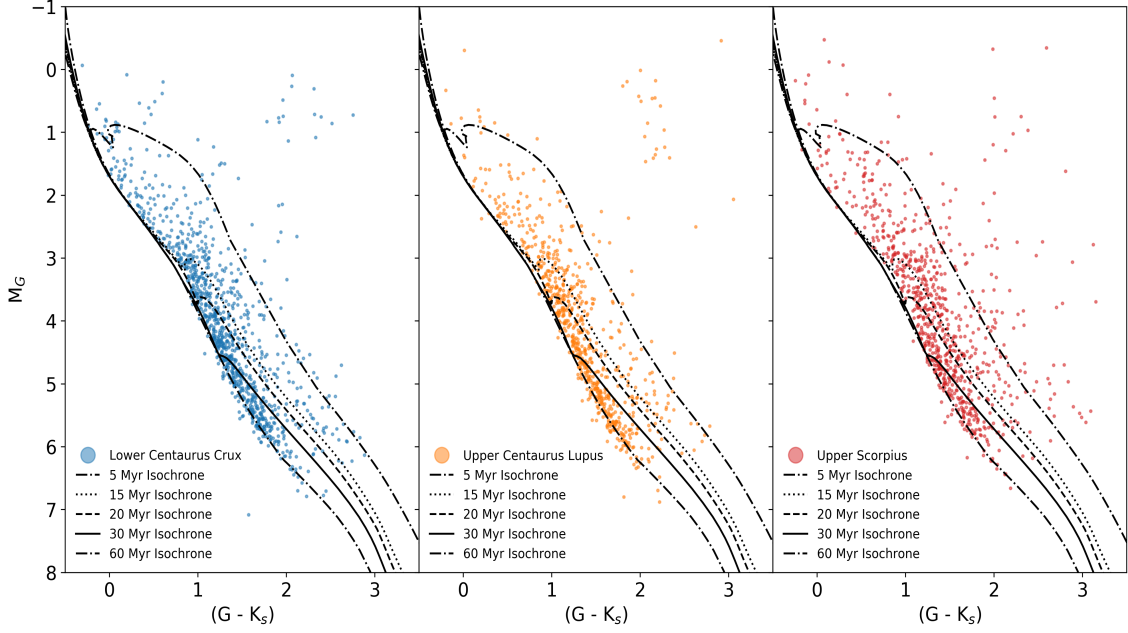


Figure 22: Something!

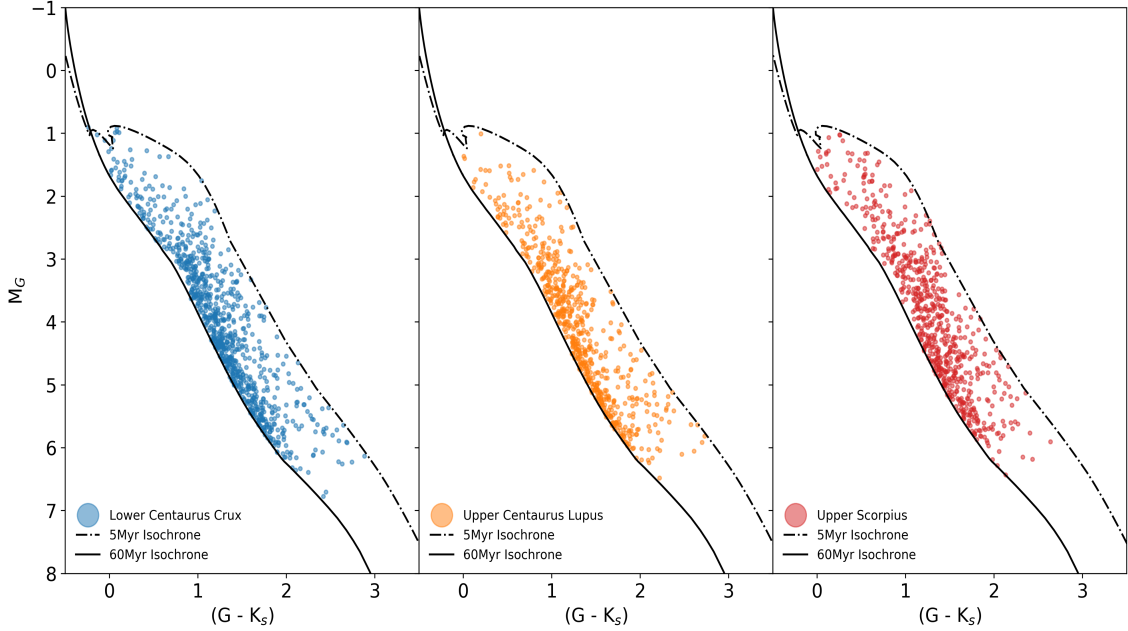


Figure 23: Something!

isochrones upwards and we will lose stars lying on the main-sequence. However, in the case of the 5-Myr isochrone, if we include extinction, then the isochrone will shift upwards including more stars that could be ruled out by our first selection method. Therefore, we proceed to compute the 5-Myr isochrone including the extinction factor. Based on observation from [de Geus et al., 1989](#), we were able to calculate the average, median and 90-percentile extinction values for each sub-region. In the case of LCC a total number of 41 stars were used, while for UCL and US, 141 and 100 stars, respectively. In [Figure 24](#), the histograms for each sub-region are shown along with the average, median, and 90-percentile extinction values. In the case of LCC and UCL, the

values are always quite similar, but in the case of US, the values are significantly higher which may affect more drastically the isochrones and stellar tracks in comparison to the other two sub-regions. The values obtained for the average, are in agreement with values reported by Wright and Mamajek, 2018 and are well correlated with the distribution of the dust, as seen in the IRAS 100 μ m map de Geus et al., 1989. These values are 0.23, 0.17, 0.76 for LCC, UCL, and US, respectively.

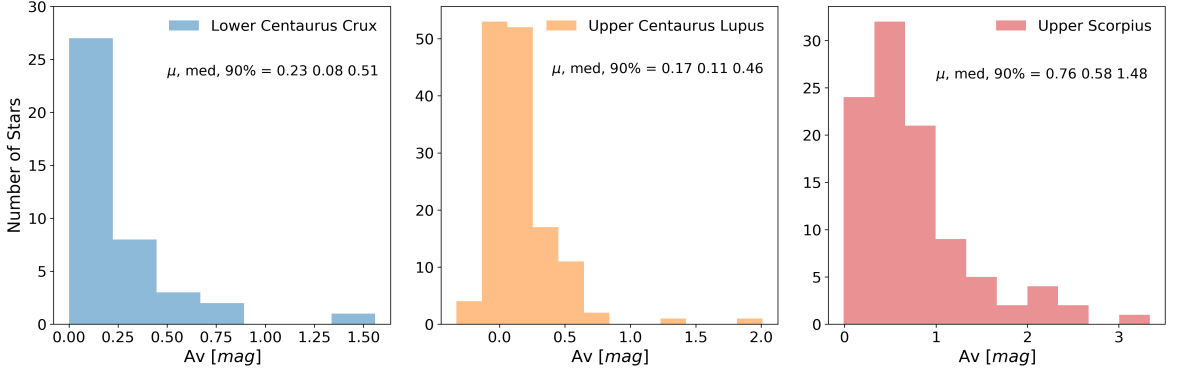


Figure 24: Something!

On top of that, the 5-Myr isochrone was computed using the average extinction values reported above to perform the selection of stars in the color-magnitude diagrams once more. As can be seen in Figure 26, the shape of the 5-Myr isochrone when introducing the extinction factor changes dramatically, moving upwards, increasing the number of stars in our selection. The same happens to LCC and UCL but in a less proportion. However, it is worth noting that the isochrones do not cross each other around $M_G \sim 1.0$ [mag] as was the case shown in Figure 22, allowing for brighter stars to be selected in our sample. If we center our view in the stellar tracks, it is evident from Figure 25 that there exists a displacement downwards. However, as stars above $2.1M_\odot$ are not a lot, and this does not change that much, we will not perform any cut in stellar mass but we will just cut in stellar age using the isochrones. The new cut and final sample using the isochrones in which the youngest isochrone is affected by extinction is shown in Figure 27.

The main goal out of this process is to obtain a reliable sample which contain as much as possible stars which could be potential candidates to belong to the Sco-Cen association based on distance and dynamical properties derived from literature. As was stated before, this analysis was performed on a sample data using *Gaia*-DR1, and the final sample is made of LCC = 889, UCL = 644, and US = 705 stars respectively, in which there is a slight increase in the number of stars per sub-region compared to the case in which no extinction is used as expected because the region between the isochrones is now larger.

3.5 LIGHT CURVES

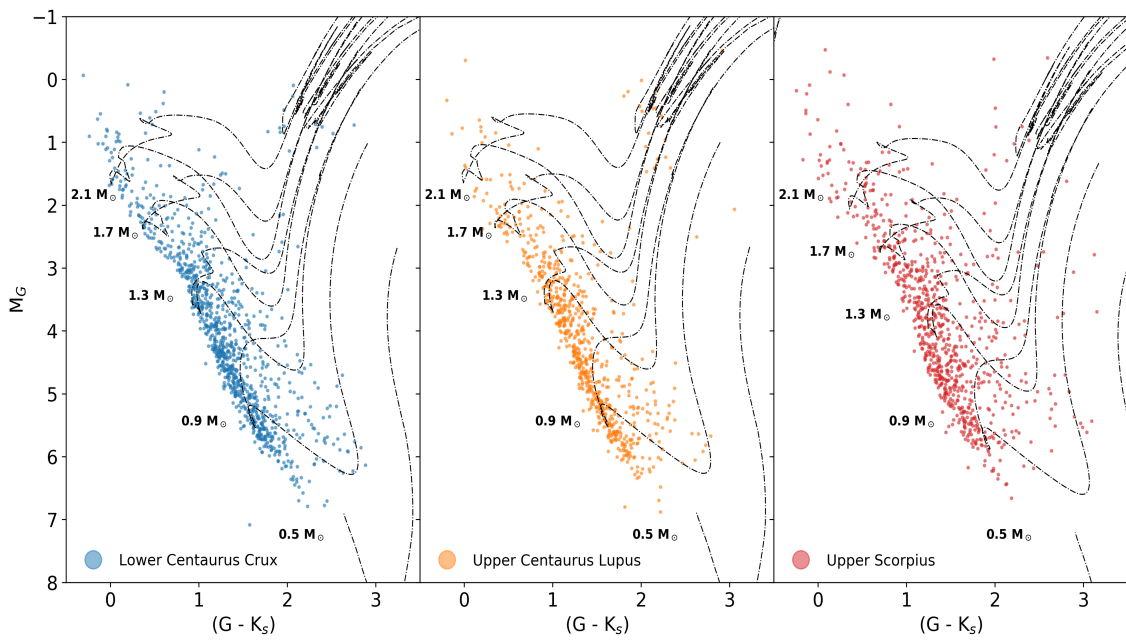


Figure 25: Something!

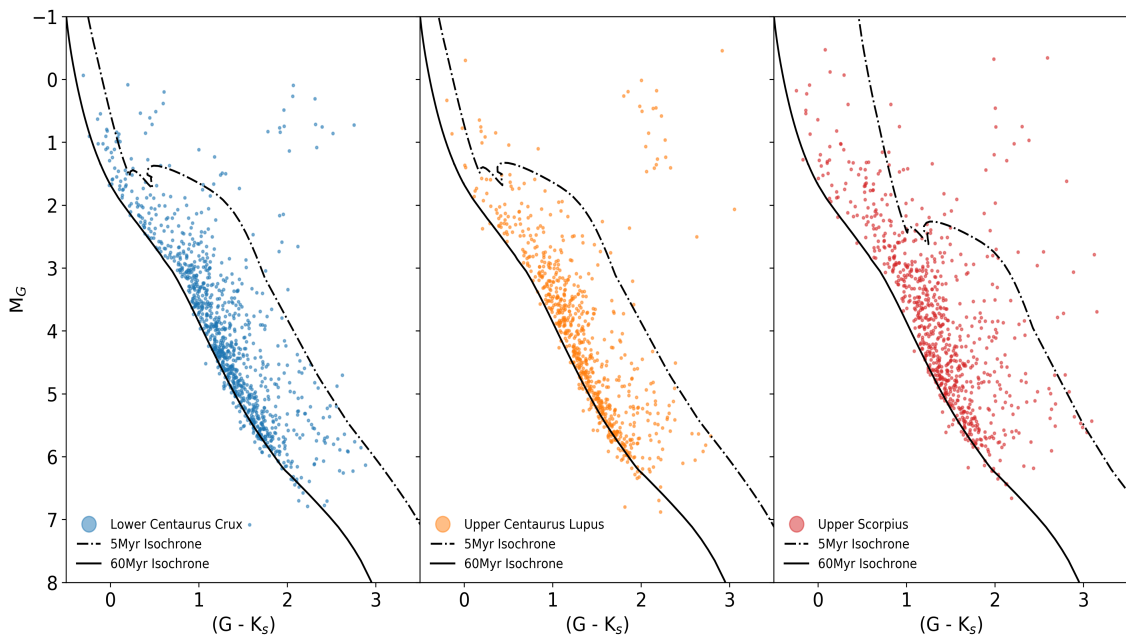


Figure 26: Something!

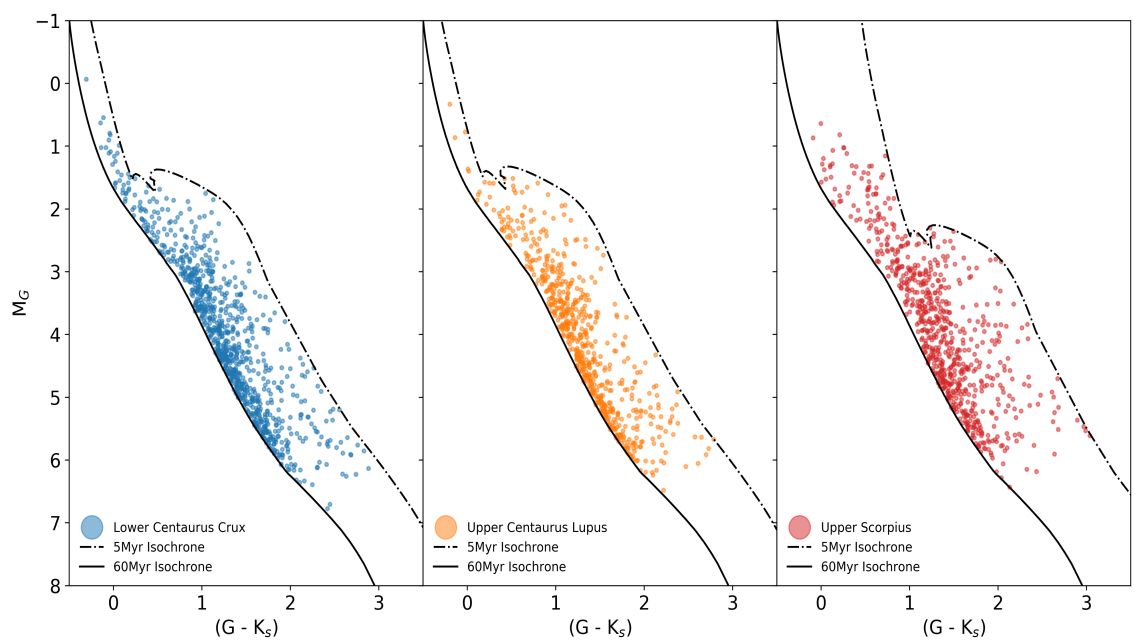


Figure 27: Something!

4

RESULTS AND DISCUSSION

4.1 INTRODUCTION

5

SUMMARY

BIBLIOGRAPHY

- [1] W. J. Borucki and A. L. Summers. The photometric method of detecting other planetary systems. *ICARUS*, 58:121–134, apr 1984. doi: 10.1016/0019-1035(84)90102-7. (Cited on page 10.)
- [2] R. P. Butler, J. T. Wright, G. W. Marcy, D. A. Fischer, S. S. Vogt, C. G. Tinney, H. R. A. Jones, B. D. Carter, J. A. Johnson, C. McCarthy, and A. J. Penny. Catalog of Nearby Exoplanets. *ApJ*, 646:505–522, jul 2006. doi: 10.1086/504701. (Cited on pages 4, 6, and 14.)
- [3] O. W. Butters, R. G. West, D. R. Anderson, A. Collier Cameron, W. I. Clarkson, B. Enoch, C. A. Haswell, C. Hellier, K. Horne, Y. Joshi, S. R. Kane, T. A. Lister, P. F. L. Maxted, N. Parley, D. Pollacco, B. Smalley, R. A. Street, I. Todd, P. J. Wheatley, and D. M. Wilson. The first WASP public data release. *A&A*, 520:L10, sep 2010. doi: 10.1051/0004-6361/201015655. (Cited on page 29.)
- [4] R. M. Canup. Origin of Saturn’s rings and inner moons by mass removal from a lost Titan-sized satellite. *Nature*, 468:943–946, dec 2010. doi: 10.1038/nature09661. (Cited on page 13.)
- [5] A. Cassan, D. Kubas, J.-P. Beaulieu, M. Dominik, K. Horne, J. Greenhill, J. Wambsganss, J. Menzies, A. Williams, U. G. Jørgensen, A. Udalski, D. P. Bennett, M. D. Albrow, V. Batista, S. Brillant, J. A. R. Caldwell, A. Cole, C. Coutures, K. H. Cook, S. Dieters, D. Dominis Prester, J. Donatowicz, P. Fouqué, K. Hill, N. Kains, S. Kane, J.-B. Marquette, R. Martin, K. R. Pollard, K. C. Sahu, C. Vinter, D. Warren, B. Watson, M. Zub, T. Sumi, M. K. Szymański, M. Kubiak, R. Poleski, I. Soszynski, K. Ulaczyk, G. Pietrzyński, and Ł. Wyrzykowski. One or more bound planets per Milky Way star from microlensing observations. *Nature*, 481:167–169, jan 2012. doi: 10.1038/nature10684. (Cited on page 9.)
- [6] S. Charnoz, L. Dones, L. W. Esposito, P. R. Estrada, and M. M. Hedman. *Origin and Evolution of Saturn’s Ring System*, page 537. 2009. doi: 10.1007/978-1-4020-9217-6_17. (Cited on page 13.)
- [7] S. Charnoz, A. Morbidelli, L. Dones, and J. Salmon. Did Saturn’s rings form during the Late Heavy Bombardment? *ICARUS*, 199:413–428, feb 2009. doi: 10.1016/j.icarus.2008.10.019. (Cited on page 13.)
- [8] J. Choi, A. Dotter, C. Conroy, M. Cantiello, B. Paxton, and B. D. Johnson. Mesa Isochrones and Stellar Tracks (MIST). I. Solar-scaled Models. *ApJ*, 823:102, jun 2016. doi: 10.3847/0004-637X/823/2/102. (Cited on pages 20 and 29.)
- [9] J. E. Colwell. The disruption of planetary satellites and the creation of planetary rings. *Planet. Space Sci.*, 42:1139–1149, dec 1994. doi: 10.1016/0032-0633(94)90013-2. (Cited on page 13.)
- [10] A. Cumming, R. P. Butler, G. W. Marcy, S. S. Vogt, J. T. Wright, and D. A. Fischer. The Keck Planet Search: Detectability and the Minimum Mass and Orbital Period Distribution of Extrasolar Planets. *PASP*, 120:531, may 2008. doi: 10.1086/588487. (Cited on pages 4, 6, and 14.)

- [11] E. J. de Geus, P. T. de Zeeuw, and J. Lub. Physical parameters of stars in the Scorpio-Centaurus OB association. *A&A*, 216:44–61, jun 1989. (Cited on pages 29, 33, and 34.)
- [12] P. T. de Zeeuw, R. Hoogerwerf, J. H. J. de Bruijne, A. G. A. Brown, and A. Blaauw. A HIPPARCOS Census of the Nearby OB Associations. *AJ*, 117:354–399, jan 1999. doi: 10.1086/300682. (Cited on page 29.)
- [13] A. Dotter. MESA Isochrones and Stellar Tracks (MIST) 0: Methods for the Construction of Stellar Isochrones. *ApJS*, 222:8, jan 2016. doi: 10.3847/0067-0049/222/1/8. (Cited on pages 20 and 29.)
- [14] Gaia Collaboration, T. Prusti, J. H. J. de Bruijne, A. G. A. Brown, A. Vallenari, C. Babusiaux, C. A. L. Bailer-Jones, U. Bastian, M. Biermann, D. W. Evans, and et al. The Gaia mission. *A&A*, 595:A1, nov 2016. doi: 10.1051/0004-6361/201629272. (Cited on page 9.)
- [15] A. W. Harris. The origin and evolution of planetary rings. In R. Greenberg and A. Brahic, editors, *IAU Colloq. 75: Planetary Rings*, pages 641–659, 1984. (Cited on page 13.)
- [16] Ing-Guey Jiang, Li-Chin Yeh, Yen-Chang Chang, and Wen-Liang Hung. On the Mass-Period Distributions and Correlations of Extrasolar Planets. *ApJ*, 134(5):2061, 2007. (Cited on pages 4, 5, and 14.)
- [17] P. Kroupa. On the variation of the initial mass function. *MNRAS*, 322:231–246, apr 2001. doi: 10.1046/j.1365-8711.2001.04022.x. (Cited on page 7.)
- [18] S. Magnussen. An algorithm for generating positively correlated Beta-distributed random variables with known marginal distributions and a specified correlation. *CMStatistics*, 46(2):397–406, feb 2004. (Cited on page 5.)
- [19] D. Nesvorný, J. L. A. Alvarellos, L. Dones, and H. F. Levison. Orbital and Collisional Evolution of the Irregular Satellites. *AJ*, 126:398–429, jul 2003. doi: 10.1086/375461. (Cited on page 10.)
- [20] E. L. Nielsen, L. M. Close, B. A. Biller, E. Masciadri, and R. Lenzen. Constraints on Extrasolar Planet Populations from VLT NACO/SDI and MMT SDI and Direct Adaptive Optics Imaging Surveys: Giant Planets are Rare at Large Separations. 41:107–110, jan 2010. doi: 10.1051/eas/1041008. (Cited on pages 4, 5, 6, 14, and 20.)
- [21] H. P. Osborn, J. E. Rodriguez, M. A. Kenworthy, G. M. Kennedy, E. E. Mamajek, C. E. Robinson, C. C. Espaillat, D. J. Armstrong, B. J. Shappee, A. Bieryla, D. W. Latham, D. R. Anderson, T. G. Beatty, P. Berlind, M. L. Calkins, G. A. Esquerdo, B. S. Gaudi, C. Hellier, T. W.-S. Holoién, D. James, C. S. Kochanek, R. B. Kuhn, M. B. Lund, J. Pepper, D. L. Pollacco, J. L. Prieto, R. J. Siverd, K. G. Stassun, D. J. Stevens, K. Z. Stanek, and R. G. West. Periodic eclipses of the young star PDS 110 discovered with WASP and KELT photometry. *MNRAS*, 471:740–749, oct 2017. doi: 10.1093/mnras/stx1249. (Cited on pages 9 and 10.)
- [22] M. J. Pecaut and E. E. Mamajek. The star formation history and accretion-disc fraction among the K-type members of the Scorpius-Centaurus OB association. *MNRAS*, 461:794–815, sep 2016. (Cited on pages 29, 30, and 32.)
- [23] A. C. Quillen and D. E. Trilling. Do Proto-jovian Planets Drive Outflows? *ApJ*, 508:707–713, dec 1998. doi: 10.1086/306421. (Cited on page 10.)

- [24] S. Rieder and M. A. Kenworthy. Constraints on the size and dynamics of the J1407b ring system. *A&A*, 596:A9, nov 2016. doi: 10.1051/0004-6361/201629567. (Cited on page 9.)
- [25] A. C. Rizzuto, M. J. Ireland, and J. G. Robertson. VizieR Online Data Catalog: Membership of Sco OB2 moving group (Rizzuto+, 2011). *VizieR Online Data Catalog*, 741, apr 2012. (Cited on page 29.)
- [26] E. E. Salpeter. The Luminosity Function and Stellar Evolution. *ApJ*, 121:161, jan 1955. doi: 10.1086/145971. (Cited on page 7.)
- [27] M. S. Tiscareno. *Planetary Rings*, page 309. 2013. doi: 10.1007/978-94-007-5606-9_7. (Cited on page 13.)
- [28] N. J. Wright and E. E. Mamajek. The Kinematics of the Scorpius-Centaurus OB Association from Gaia DR1. *MNRAS*, jan 2018. doi: 10.1093/mnras/sty207. (Cited on pages 29 and 34.)
- [29] S. Zucker and T. Mazeh. On the Mass-Period Correlation of the Extrasolar Planets. *ApJL*, 568: L113–L116, apr 2002. doi: 10.1086/340373. (Cited on pages 4 and 5.)

APPENDIX

6.1 SQL-QUERIES

In this section, the queries performed in the *Gaia* database are shown for the three different fields of Sco-Cen OB Association namely Lower Centaurus Crux (LCC), Upper Centaurus Lupus (UCL), and Upper Scorpius (US).

Lower Centaurus Crux (LCC)

```
SELECT gaia.source_id,
gaia.ra, gaia.ra_error, gaia.dec, gaia.dec_error, gaia.parallax, gaia.parallax_error
, gaia.l, gaia.b,
gaia.phot_g_mean_mag+5*log10(gaia.parallax)-10 AS g_mag_abs,
tycho2.bt_mag-tycho2.vt_mag AS b_min_v
FROM gaiadr1.tgas_source AS gaia
INNER JOIN tycho2 AS tycho2
ON gaia.tycho2_id = tycho2.id
WHERE gaia.parallax >= 6 AND gaia.parallax <= 12 AND gaia.b >= -10 AND gaia.b <= 16
AND gaia.l >= 285 AND gaia.l <= 313

SELECT gaia.source_id,
gaia.ra, gaia.ra_error, gaia.dec, gaia.dec_error, gaia.parallax, gaia.parallax_error
, gaia.l, gaia.b,
gaia.phot_g_mean_mag+5*log10(gaia.parallax)-10 AS g_mag_abs,
gaia.phot_g_mean_mag-tmass.ks_m AS g_min_ks, gaia.pmra, gaia.pmra_error, gaia.pmdec,
gaia.pmdec_error
FROM gaiadr1.gaia_source AS gaia INNER JOIN gaiadr1.tmass_best_neighbour AS xmatch
ON gaia.source_id = xmatch.source_id
INNER JOIN gaiadr1.tmass_original_valid AS tmass ON tmass.tmass_oid = xmatch.
tmass_oid
WHERE gaia.parallax >= 6 AND gaia.parallax <= 12 AND gaia.b >= -10 AND gaia.b <= 16
AND gaia.l >= 285 AND gaia.l <= 313
AND gaia.pmra < 10 AND gaia.pmdec < 30 AND sqrt(power(gaia.pmra,2)+power(gaia.pmdec,
,2)) > 15 AND sqrt(power(gaia.pmra,2)+power(gaia.pmdec,2)) < 55
```

Upper Centaurus Lupus (UCL)

```
SELECT gaia.source_id,
gaia.ra, gaia.ra_error, gaia.dec, gaia.dec_error, gaia.parallax, gaia.parallax_error
, gaia.l, gaia.b,
gaia.phot_g_mean_mag+5*log10(gaia.parallax)-10 AS g_mag_abs,
tycho2.bt_mag-tycho2.vt_mag AS b_min_v
FROM gaiadr1.tgas_source AS gaia
INNER JOIN tycho2 AS tycho2
```

```

ON gaia.tycho2_id = tycho2.id
WHERE gaia.parallax >= 6.0 AND gaia.parallax <= 12 AND gaia.b >= 5 AND gaia.b <= 31
    AND gaia.l >= 313 AND gaia.l <= 337

SELECT gaia.source_id,
gaia.ra, gaia.ra_error, gaia.dec, gaia.dec_error, gaia.parallax, gaia.parallax_error
    , gaia.l, gaia.b,
gaia.phot_g_mean_mag+5*log10(gaia.parallax)-10 AS g_mag_abs,
gaia.phot_g_mean_mag-tmass.ks_m AS g_min_ks, gaia.pmra, gaia.pmra_error, gaia.pmdec,
    gaia.pmdec_error
FROM gaiadr1.gaia_source AS gaia INNER JOIN gaiadr1.tmass_best_neighbour AS xmatch
    ON gaia.source_id = xmatch.source_id
INNER JOIN gaiadr1.tmass_original_valid AS tmass ON tmass.tmass_oid = xmatch.
    tmass_oid
WHERE gaia.parallax >= 6.0 AND gaia.parallax <= 12 AND gaia.b >= 5 AND gaia.b <= 31
    AND gaia.l >= 313 AND gaia.l <= 337
AND gaia.pmra < 10 AND gaia.pmdec < 30 AND sqrt(power(gaia.pmra,2)+power(gaia.pmdec
    ,2)) > 12 AND sqrt(power(gaia.pmra,2)+power(gaia.pmdec,2)) < 55

```

Upper Scorpius (US)

```

SELECT gaia.source_id,
gaia.ra, gaia.ra_error, gaia.dec, gaia.dec_error, gaia.parallax, gaia.parallax_error
    , gaia.l, gaia.b,
gaia.phot_g_mean_mag+5*log10(gaia.parallax)-10 AS g_mag_abs,
tycho2.bt_mag-tycho2.vt_mag AS b_min_v
FROM gaiadr1.tgas_source AS gaia
INNER JOIN tycho2 AS tycho2
ON gaia.tycho2_id = tycho2.id
WHERE gaia.parallax >= 6.0 AND gaia.parallax <= 12 AND gaia.b >= 7 AND gaia.b <= 32
    AND gaia.l >= 337 AND gaia.l <= 360

SELECT gaia.source_id,
gaia.ra, gaia.ra_error, gaia.dec, gaia.dec_error, gaia.parallax, gaia.parallax_error
    , gaia.l, gaia.b,
gaia.phot_g_mean_mag+5*log10(gaia.parallax)-10 AS g_mag_abs,
gaia.phot_g_mean_mag-tmass.ks_m AS g_min_ks, gaia.pmra, gaia.pmra_error, gaia.pmdec,
    gaia.pmdec_error
FROM gaiadr1.gaia_source AS gaia INNER JOIN gaiadr1.tmass_best_neighbour AS xmatch
    ON gaia.source_id = xmatch.source_id
INNER JOIN gaiadr1.tmass_original_valid AS tmass ON tmass.tmass_oid = xmatch.
    tmass_oid
WHERE gaia.parallax >= 6.0 AND gaia.parallax <= 12 AND gaia.b >= 7 AND gaia.b <= 32
    AND gaia.l >= 337 AND gaia.l <= 360
AND gaia.pmra < 10 AND gaia.pmdec < 30 AND sqrt(power(gaia.pmra,2)+power(gaia.pmdec
    ,2)) < 47

```

6.2 SAMPLE SELECTION

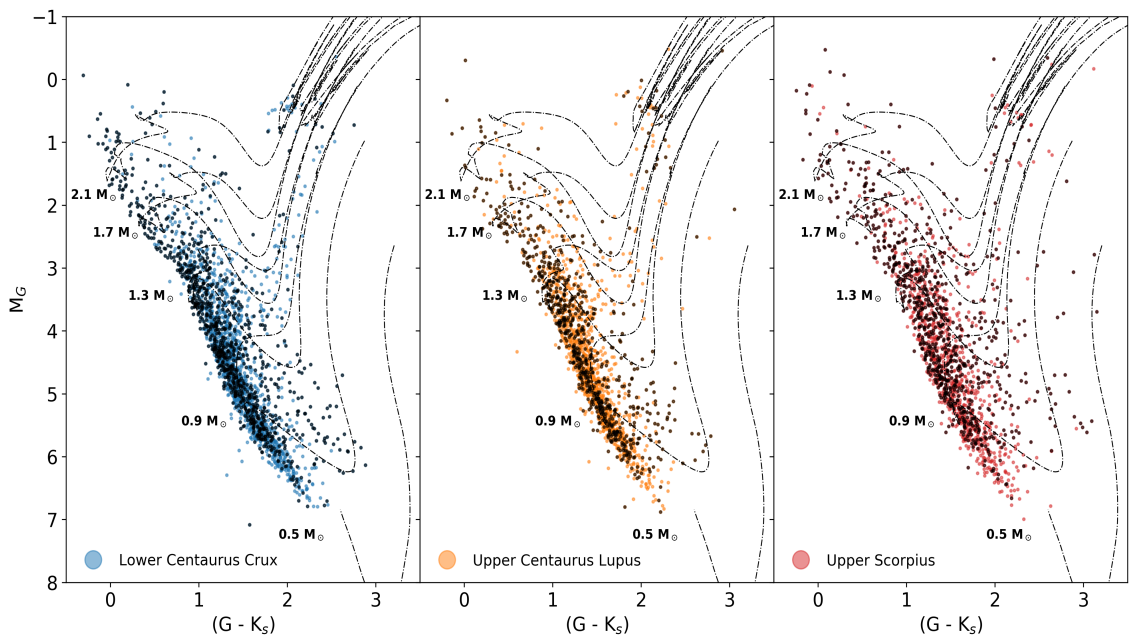


Figure 28: Something!

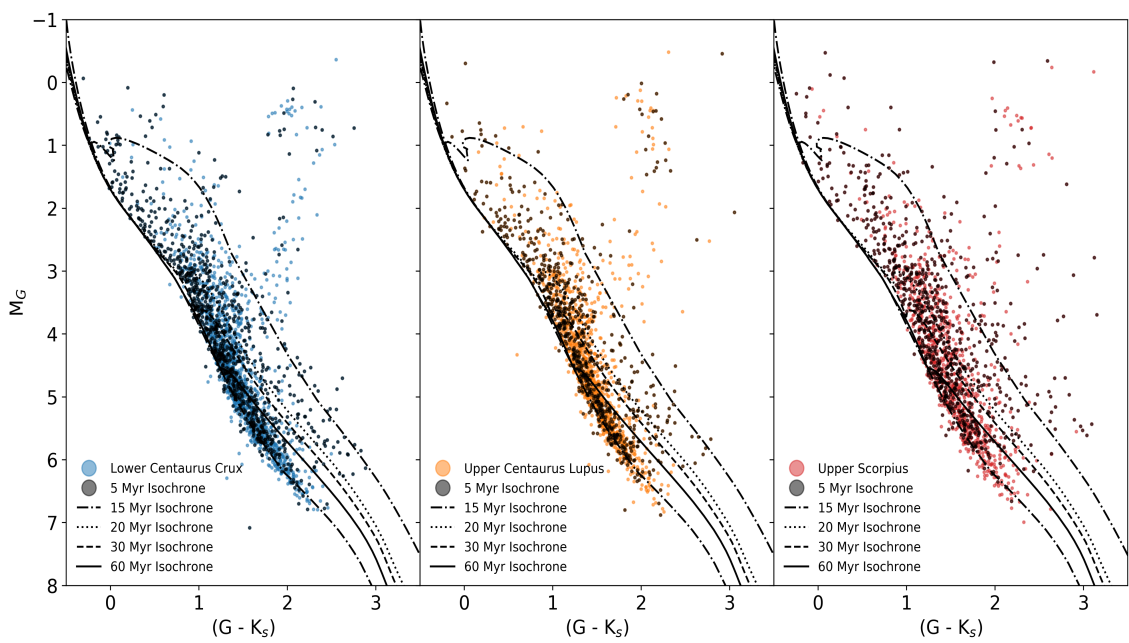


Figure 29: Something!